Available online at www.sciencedirect.com

ScienceDirect

Geochimica et Cosmochimica Acta 196 (2017) 36–57

Geochimica et Cosmochimica Acta

www.elsevier.com/locate/gca

Deep mixing of mantle melts beneath continental flood basalt provinces: Constraints from olivine-hosted melt inclusions in primitive magmas

Eleanor S. Jennings [a,*], Sally A. Gibson [a], John Maclennan [a], Jussi S. Heinonen [b,1]

[a] Department of Earth Sciences, University of Cambridge, Downing Street, Cambridge CB2 3EQ, United Kingdom
[b] Finnish Museum of Natural History, P.O. Box 44, University of Helsinki, 00014 Helsinki, Finland

Received 21 March 2016; accepted in revised form 15 September 2016; available online 22 September 2016

Abstract

We present major and trace element compositions of 154 re-homogenised olivine-hosted melt inclusions found in primitive rocks (picrites and ferropicrites) from the Mesozoic Paraná–Etendeka and Karoo Continental Flood Basalt (CFB) provinces. The major element compositions of the melt inclusions, especially their Fe/Mg ratios, are variable and erratic, and attributed to the re-homogenisation process during sample preparation. In contrast, the trace element compositions of both the picrite and ferropicrite olivine-hosted melt inclusions are remarkably uniform and closely reflect those of the host whole-rocks, except in a small subset affected by hydrothermal alteration. The Paraná–Etendeka picrites and ferropicrites are petrogenetically related to the more evolved and voluminous flood basalts, and so we propose that compositional homogeneity at the melt inclusion scale implies that the CFB parental mantle melts were well mixed prior to extensive crystallisation.

The incompatible trace element homogeneity of olivine-hosted melt inclusions in Paraná–Etendeka and Karoo primitive magmatic rocks has also been identified in other CFB provinces and contrasts with findings from studies of basalts from mid-ocean ridges (e.g. Iceland and FAMOUS on the Mid Atlantic Ridge), where heterogeneity of incompatible trace elements in olivine-hosted melt inclusions is more pronounced. We suggest that the low variability in incompatible trace element contents of olivine-hosted melt inclusions in near-primitive CFB rocks, and also ocean island basalts associated with moderately thick lithosphere (e.g. Hawaii, Galápagos, Samoa), may reflect mixing along their longer transport pathways during ascent and/or a temperature contrast between the liquidus and the liquid when it arrives in the crust. These thermal paths promote mixing of mantle melts prior to their entrapment by growing olivine crystals in crustal magma chambers. Olivine-hosted melt inclusions of ferropicrites from the Paraná–Etendeka and Karoo CFB have the least variable compositions of all global melt inclusion suites, which may be a function of their unusually deep origin and low viscosity.

Keywords: Continental flood basalt; Melt inclusion; Mixing; Paraná-Etendeka; Karoo

1. INTRODUCTION

1.1. The melt inclusion record of compositional heterogeneity in magmas

Fractional melting of adiabatically upwelling mantle produces instantaneous melts with highly variable compositions. This compositional variability contrasts strongly with

* Corresponding author at: Bayerisches Geoinstitut, Universität Bayreuth, 95440 Bayreuth, Germany.
E-mail addresses: eleanor.jennings@uni-bayreuth.de (E.S. Jennings), sally@esc.cam.ac.uk (S.A. Gibson), jcm1004@cam.ac.uk (J. Maclennan), jussi.s.heinonen@helsinki.fi (J.S. Heinonen).
[1] Present address: Department of Geosciences and Geography, P.O. Box 64, University of Helsinki, 00014 Helsinki, Finland.

http://dx.doi.org/10.1016/j.gca.2016.09.015
0016-7037/

the relatively homogeneous chemistry often displayed by suites of lava flows and sometimes extensive volcanic successions (e.g. Cox, 1980; Erlank et al., 1984; Arndt et al., 1993; Wooden et al., 1993; Reidel and Tolan, 2013). A link to processes operating deeper within igneous plumbing systems is provided by olivine-hosted melt inclusions. Melt inclusions represent tiny droplets of liquid trapped by growing crystals and are important because their isolation from the surrounding melt preserves the liquid composition at the time of entrapment. Olivine-hosted melt inclusions from primitive magmatic rocks are of particular interest because they contain important information about how diverse mantle melts combine, homogenise and crystallise within a single magmatic plumbing system.

In oceanic settings, olivine-hosted melt inclusions from primitive magmas frequently display a large variability in incompatible trace element concentrations and ratios. This was first noted in melt inclusions from mid-ocean ridge basalts (MORB) by Sobolev and Shimizu (1993), who attributed the variability to fractional melting in the mantle. Similar observations and interpretations have subsequently been made for ocean island basalts (OIBs) and on Iceland (e.g. Gurenko and Chaussidon, 1995; Sobolev, 1996; Shimizu, 1998; Slater et al., 2001; Norman et al., 2002; Sours-Page et al., 2002; Maclennan et al., 2003; Maclennan, 2008a). Variability has also been identified in the Pb and Sr radiogenic isotopic ratios of olivine-hosted melt inclusions; such variations cannot be attributed to melting processes and indicate high amplitude, short length scale isotopic heterogeneity in the mantle source regions of basalts erupted from individual volcanoes (Saal et al., 1998; Jackson and Hart, 2006; Maclennan, 2008b; Sobolev et al., 2011; Sakyi et al., 2012). As a consequence of studies such as these, incompatible trace element variability in both lavas and melt inclusions has often been interpreted as a product of both mantle melting process and compositional heterogeneity in the source (e.g. Norman et al., 2002; Stracke et al., 2003b; Sobolev et al., 2000, 2011; Rudge et al., 2013). Compositional heterogeneity in mantle melts is quickly destroyed by convective mixing, e.g. in lower crustal sills, but when this process is concurrent with crystallisation it may be captured by the melt inclusion record (Maclennan, 2008a). Although well-established in Iceland (Maclennan et al., 2003; Maclennan, 2008a; Neave et al., 2013), the controls over the timing of convective mixing relative to crystallisation of mantle melts are not well understood at other locations.

In this study, we present analyses of 154 olivine-hosted melt inclusions from primitive olivine-rich rocks from the Paraná–Etendeka and Karoo Continental Flood Basalt (CFB) provinces. These high-MgO rocks are scarce in CFB provinces because extensive crystal fractionation in deep and complex crustal plumbing systems typically produces more evolved magmas with rather monotonous major element compositions (Fig. 1; from the GEOROC database, Sarbas and Nohl, 2008). Nevertheless, if primitive magmas are able to ascend rapidly and bypass large crustal magma chambers, they have the potential to preserve evidence of geochemical variability of the initial mantle melts involved in CFB genesis. The original thick lithosphere beneath CFB provinces limits adiabatic decompression melting in the convecting mantle and further increases the possibility of detecting a geochemical signal of lithological heterogeneity in early-formed magmas, such as those generated by deep melting of pyroxenite and/or peridotite. Moreover, olivine-hosted melt inclusions found in primitive magmatic rocks have the added advantage of preserving initial melts in a relatively closed system and hence provide a window through subsequent crystal fractionation, assimilation and hydrothermal alteration processes that may compromise whole rock data.

Analyses of olivine-hosted melt inclusions have been published from several CFB provinces including: Paraná–Etendeka, North Atlantic, Yemen, Emeishan and Siberian Traps (Kent et al., 2002; Yaxley et al., 2004; Nielsen et al., 2006; Sobolev et al., 2009; Keiding et al., 2011; Kamenetsky et al., 2012; Peate et al., 2012; Starkey et al., 2012). In comparison to other tectonic settings, however, the number of published analyses for primitive magmas in CFB provinces is relatively small. Our new major and trace element data for olivine-hosted melt inclusions in the Paraná–Etendeka and Karoo CFB provinces builds on these previous studies and is focused on two types of high-MgO magmatic rocks: picrite and ferropicrite. These distinct magma compositions are thought to reflect melting of peridotite and pyroxenite, respectively, within elevated temperature mantle upwelling beneath lithosphere of varying thickness (Gibson et al., 2000; Thompson et al., 2001; Gibson, 2002; Tuff et al., 2005; Heinonen and Luttinen, 2008; Heinonen et al., 2013). We compare our new incompatible trace element analyses for olivine-hosted melt inclusions with those from other CFB provinces, and the much larger global database of OIB and MORB, in order to examine the role of the lithosphere and tectonic setting on melt inclusion chemical variability and the relative timing of mantle melt mixing and crystallisation.

1.2. Primitive mantle melts in CFB provinces

Continental flood basalts constitute a major portion of subaerial Large Igneous Provinces (LIPs). The individual CFB successions consist of enormous volumes of magma ($>10^5$ km^3, Bryan and Ernst, 2008) with the bulk of lava piles being erupted over very short timescales ($<\sim$1–5 Myr, Courtillot and Renne, 2003). The rapid production of vast volumes of melt in CFB provinces has generally been linked to adiabatic decompression melting of mantle plume heads impacting beneath rifting lithosphere (Richards et al., 1989; White and McKenzie, 1989). Small volumes of near-primitive, non-cumulate Mg-rich rocks are found in CFB provinces as shallow dykes and sills or thin lava flows. Some of these rocks, known as ferropicrites, have higher FeO_T (>13 wt.%) and lower Al_2O_3 contents (typically <10 wt.%) than true picrites (Gibson et al., 2000; Riley et al., 2005; Heinonen and Luttinen, 2008). Although ferropicrites in general contain olivines with a lower forsterite content (Fo $\leqslant$ 86) than those in picrites (Fo $\leqslant$ 93; Fig. 2), they have similar Ni concentrations

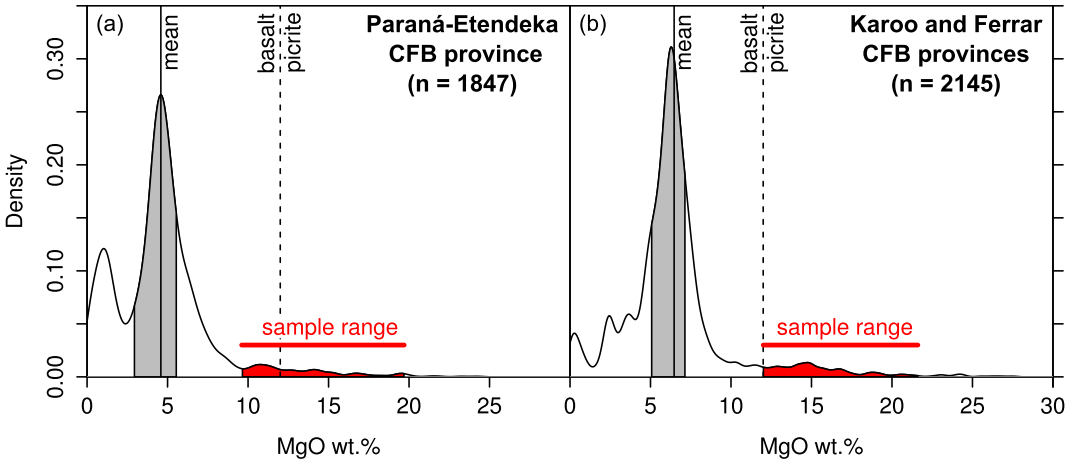

Fig. 1. Kernel density plot showing the probability distribution of MgO wt.% in whole-rock and glass analyses of samples from the GEOROC database (Sarbas and Nohl, 2008), excluding exotic compositions, from (a) the Paraná–Etendeka CFB province and (b) the Karoo and Ferrar CFB provinces. The peak at around 5 wt.% MgO is a result of sampling of the voluminous flood basalts; for context, the whole-rock MgO range of samples of this study is shown by the red bar. Boundary between basalt and picrite at 12 wt.% MgO is from Le Bas (2000). Grey region shows lower and upper quartile.

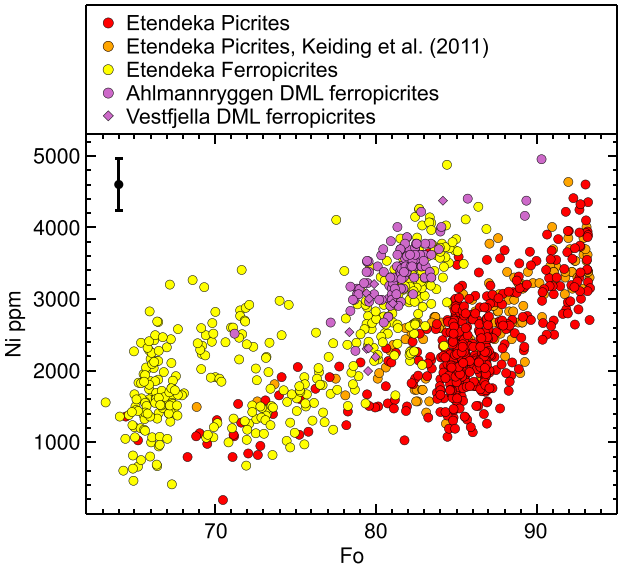

Fig. 2. Ni content of olivine phenocrysts in Horingbaai picrites (red filled circles, this study and Thompson et al., 2001; orange filled circles, Keiding et al., 2011), Etendeka ferropicrites (yellow filled circles, this study and Gibson et al., 2000) and Dronning Maud Land ferropicrites (purple filled circles, Ahlmannryggen samples, this study and Heinonen et al., 2013; purple filled diamonds, Vestfjella samples, this study). Black point shows typical $\pm 1\sigma$ error from repeat analyses. (For interpretation of the references to colour in this figure legend, the reader is referred to the web version of this article.)

and are thought to represent primitive plume-derived mantle melts with elevated Fe/Mg (Gibson et al., 2000; Jennings, 2016). The unusual bulk-rock chemistry of primitive ferropicrites has been used to argue that they form by melting of a garnet pyroxenite source (Gibson, 2002; Tuff et al., 2005; Heinonen et al., 2013, 2014; Jennings, 2016). While ferropicritic melts are not likely to be the dominant parental melt to the majority of the voluminous CFBs (e.g. Luttinen et al., 2015), it is possible that similar liquids are part of the range of primary melt compositions that mix to form the parental liquids of CFBs. Only one previous study has presented melt inclusion data from ferropicrites (Gudchikhinsky formation of the Siberian Traps; Sobolev et al., 2009) although the authors did not focus on the anomalously high FeO_T contents of their samples.

2. SAMPLES

The whole-rock compositions of lavas from both the Paraná–Etendeka and Karoo CFB provinces exhibit large frequency peaks at 4–6 wt.% MgO, due to the prevalence of basaltic compositions in these provinces (Fig. 1). The rocks analysed in this study are lavas and hypabyssal intrusions from the high-MgO tail of the probability distribution shown in Fig. 1. Those with the highest whole-rock MgO are thought to have undergone some olivine accumulation but the high Ni content of olivine phenocrysts from these samples ($\leqslant\sim$4000 ppm, Fig. 2) confirms their origin as primitive mantle-derived melts. While minor hydrothermal alteration has affected some of the samples used in our study (as evident by chlorite in the groundmass and the partial serpentinisation of olivine), unaffected olivine cores still preserve pristine melt inclusions.

2.1. Paraná–Etendeka CFB province

Early Cretaceous (132–133 Ma) picrites and ferropicrites are found as dykes, sills and flows in the Etendeka region of NW Namibia. This is part of the Paraná–Etendeka CFB sequence that is associated with rifting of Africa and South America (Thompson et al., 2001; Gibson, 2002). Picritic dykes found near Horingbaai contain olivine phenocrysts

that are 1–2 mm in length and have cores in the compositional range Fo_{86-93}. The co-existence of olivine with occasional phenocrysts of plagioclase feldspar places initial crystallisation of the picrites at moderately low pressures in the upper crust (Thompson et al., 2001). Whole-rock incompatible trace element ratios indicate that the Horingbaai picrites have assimilated small amounts (0–6%) of local K-feldspar-rich upper crust, but generally the isotopic ratios suggest a dominantly sublithospheric melt source region (e.g. initial ε_{Nd} from +3.7 to +8.7 at 132 Ma; Thompson et al., 2001). This is confirmed with $\delta^{18}O$ measurements by Harris et al. (2015), who found that phenocrysts from similar Horingbaai picrites have mantle-like to slightly contaminated values that correlate with whole-rock Sr, Nd and Pb isotopic ratios.

Although no direct equivalent of the Horingbaai-type picrites is represented in the erupted main Etendeka CFB succession, their spatial and temporal association with the CFB units suggests that they were part of the plumbing system of the province (Marsh et al., 2001). Given their likely origin from the same mantle source, the Horingbaai picrites should have similar characteristics to the melts parental to the CFBs. The ages of the Horingbaai dykes are constrained by field relationships (Thompson et al., 2001): they cross-cut a thick sill dated at 131 ± 1.9 Ma and 132 ± 0.7 Ma (Renne et al., 1996; Kirstein et al., 2001), but are truncated by a granite intrusion with an age of around 131 Ma (Schmitt et al., 2000). They therefore formed towards the end of the main flood basalt emplacement but well within the age range of the province as a whole (Gibson et al., 2006). The parental melts of the Horingbaai dykes are thought to have formed from adiabatic decompression of upwelling peridotite in the proto-Tristan plume, at mantle potential temperatures (T_P) of 1470 to 1560 °C, beneath moderately thick (55–95 km) lithosphere (Thompson et al., 2001). We note that some samples grouped as picrites are strictly basalts (97SB29, 97SB46, 97SB62, 97SB75) but these all have MgO ⩾ 9.6 wt.%.

The Etendeka ferropicrites are highly olivine-phyric. Some samples contain only pristine olivine, whereas others contain olivine with minor secondary alteration: they are partially serpentinised or, in the case of samples 97SB67 and 97SB68, have red surface veneers of haematite or iddingsite. The presence of phenocrysts of augite is taken as evidence that some of these magmas initially crystallised in the lower crust (Gibson et al., 2000). A high proportion of oxide phases are common in the ferropicrite groundmass. We note that one sample (97SB80) contains <12 wt.% MgO and is strictly a ferrobasalt. Most Etendeka ferropicrites have fairly smooth normalised incompatible trace element patterns and are not thought to be significantly contaminated by crustal or lithospheric mantle material (Gibson et al., 2000). They have varied and somewhat lower initial ε_{Nd} than the Horingbaai picrites (−2.9 to +3.7). The ferropicrites occur at the base of the main CFB sequence and represent the first evidence of magmatic activity associated with the sub-lithospheric impact of the proto-Tristan plume (Gibson et al., 2000); their small volume and unusual chemistry means that they are not a parental melt to the main Etendeka CFB lavas.

2.2. Karoo CFB province

Ferropicrites occur as dykes at Ahlmannryggen and Vestfjella in Dronning Maud Land, Antarctica, where part of the Jurassic (~180–190 Ma) Karoo CFB province is exposed (Jourdan et al., 2005; Luttinen et al., 2015). The four samples included in this study represent two different types of ferropicrite: three of the samples are Group 3 'depleted' ferropicrites from Ahlmannryggen, which have low concentrations of highly incompatible trace elements, high near-identical initial ε_{Nd} (+7 at 180 Ma; Riley et al., 2005), and slightly higher $\delta^{18}O$ than mantle values (Harris et al., 2015); the fourth sample is an 'enriched' ferropicrite from Vestfjella with greater incompatible trace element concentrations and a lower Nd isotopic composition ($\varepsilon_{Nd} = +3.5$; Heinonen et al., 2010). Two similar Group 3 Dronning Maud Land samples yielded only slightly higher $\delta^{18}O$ than mantle values (Harris et al., 2015). A third Karoo magma type that contains ferropicrite samples (depleted ferropicrites and meimechites of Vestfjella; Heinonen and Luttinen, 2008; Heinonen et al., 2010) was not sampled for this study.

The studied Dronning Maud Land ferropicrites are fresh with abundant olivine phenocrysts (Fo_{77-86}). The Ahlmannryggen ferropicrites also contain orthopyroxene phenocrysts; they are sometimes in isolation but more commonly show a resorption texture and are mantled by clinopyroxene, which reflect an initially high pressure (>6 kbar) and perhaps polybaric, multi-stage crystallisation history (Heinonen et al., 2013). Modelling of the Nd, Sr, Pb and Os isotopic compositions of the Ahlmannryggen ferropicrites indicates that they originated by melting of a mixture of recycled crust and depleted mantle, and assimilated less than 1% Archaean crust during transit to the surface (Heinonen et al., 2014). The enriched ferropicrite from Vestfjella also likely originated from a recycled source, possibly containing sedimentary and/or metasomatic components (Heinonen et al., 2010).

2.3. Olivine-hosted melt inclusions

Although chromian spinel is the highest temperature liquidus phase in both the picrites and ferropicrites (as evidenced by their ubiquity as inclusions in olivine cores), olivine is the first volumetrically significant phase to crystallise, so that the most forsteritic olivines should trap melts with compositions that approximate the initial primary liquid compositions (e.g. Sobolev, 1996). The olivine-hosted melt inclusions examined in this study are partially to fully crystalline, which reflects their moderately slow cooling history and is consistent with the doleritic textures of their host rocks (Fig. 3a, b, d and e). The morphologies of crystals that grew post-entrapment within the melt inclusions vary from equant to elongate to dendritic or spinifex, consistent with deeper olivine crystallisation and shallow emplacement in dykes. The mineral assemblage of the inclusions is the same as the rock groundmass, with varying proportions of daughter olivine on inclusion rims, clinopyroxene, orthopyroxene, plagioclase and oxide phases. An irregular void from the original

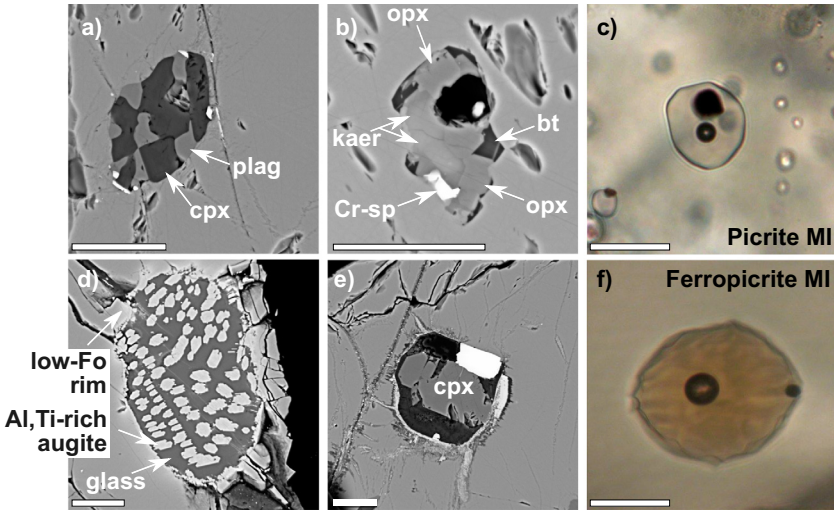

Fig. 3. Olivine-hosted melt inclusions from Etendeka samples, scale bars all 20 μm. (a) Ferropicrite melt inclusion pre-homogenisation bearing plagioclase and clinopyroxene (sample 97SB67). (b) Ferropicrite melt inclusion pre-homogenisation bearing hydrous phases (kaersutite and biotite) as well as Cr-spinel, orthopyroxene and a void which once contained a vapour bubble (sample 97SB80). (c) Picrite melt inclusion post-homogenisation consisting of glass, a vapour bubble and Cr-spinel. (d) Picrite melt inclusion pre-homogenisation containing Al and Ti-rich augite and a low Fe and Mg glass (sample 97SB34). The alignment of augite suggests that a small number of spinifex crystals are present, formed through fast cooling at the olivine edge. A clear rim of Fe-rich olivine is seen around the inclusion. (e) A breached inclusion, pre-homogenisation; secondary phases fill fractures, hydrous phases occupy the dark area, and the Cr-sp appears replaced by haematite (sample 97SB67). (f) Ferropicrite melt inclusion post-homogenisation; the glass often has a darker colour than in picrite melt inclusions. (a), (b), (d) and (e) are BSE images; (c) and (f) are photomicrographs. Abbreviations: cpx, clinopyroxene; opx, orthopyroxene; plag, plagioclase; kaer, kaersutite; bt, biotite; sp, spinel; Fo, forsterite; MI, melt inclusion.

shrinkage bubble is often seen in the melt inclusions. Many also contain chromian spinels that were trapped alongside the melt and do not disappear during re-homogenisation (Fig. 3b and c). This association reflects the heterogeneous trapping of the melt and the liquidus phase (e.g. spinel on an olivine growth surface may cause a melt-trapping cavity to form). Amphibole (kaersutite) and biotite were found in a single Etendeka ferropicrite melt inclusion (Fig. 3b). Kaersutite is also found in the groundmass of the Vestfjella ferropicrite sample and indicates that the primitive ferropicrite melt may have contained up to 1–2 wt.% water (Heinonen et al., 2010). Hydrous phases are otherwise not seen in the whole-rock samples.

3. ANALYTICAL TECHNIQUES

Samples were prepared in the Dept. of Earth Sciences at the University of Cambridge. They were crushed in a jaw crusher or by hand. Hand-picked 250–500 μm fragments of olivine containing 5–40 μm diameter inclusions were then heated in a controlled-atmosphere furnace in order to remelt the inclusions. Batches of grains were wrapped in Pt foil, placed in a Pt crucible and held at a fixed temperature for 20 min, then quenched in water. Oxygen fugacity was fixed at FMQ-1 with a $CO–CO_2$ mixture to prevent olivine oxidation. The inclusions were originally up to 100% crystalline and the homogenisation temperature is defined as the temperature required for complete loss of crystals in the inclusion, determined visually from small volume experiments at 40 °C intervals. In order to reduce the impact of overheating on diffusion rates and olivine melting, we used the minimum homogenisation temperature. This ranged from 1200 to 1280 °C for the different samples and is in agreement with Danyushevsky et al. (2002) but lower than that used by Keiding et al. (2011), who heated olivines from Paraná–Etendeka picrites at 1350 °C for 15 min. Following heating, the olivine grains were mounted in 1-inch diameter epoxy stubs and ground to an arbitrary depth, exposing a random selection of re-homogenised melt inclusions. Inclusions were selected to ensure pre-homogenisation inclusion integrity based upon their regular shape, absence of alteration associated with fractures, and lack of an excessively large bubble (Nielsen et al., 1998) and size (>15 μm).

Major element analysis was performed on a Cameca-SX100 electron probe microanalyser (EPMA) in wavelength-dispersive mode at the Dept. of Earth Sciences, University of Cambridge, with an accelerating voltage of 15 keV, a 6 nA, 5 μm beam, and a standard set of primary and secondary standards. Host olivines were analysed with a focussed 10–20 nA beam, at least 20 μm away from the rim of any melt inclusion. Major element data were collected from 365 inclusions (see Supplementary Table A1).

Rare earth elements (REE), Rb, Ba, Sr, K, Nb, Ti, Zr, Y and Sc were analysed by secondary ion mass spectrometry (SIMS) using the Cameca IMS-4f ion microprobe at the NERC Ion Microprobe Facility at the University of Edinburgh over two sessions, 12 months apart. Inclusions were bombarded with a 15 kV primary O^- ion beam, with a secondary voltage of 4500 V minus an offset of 75 V. The beam

current used was 3–5 nA, with a spot size of approximately 15 μm. Peak positions were verified before each analysis; mass 130.5 was measured as background in each cycle and was always zero. Six analytical cycles were used per analysis. NIST-610 (Jochum et al., 2011) was the primary calibration standard, and was used to correct for daily machine drift, where the maximum drift was 16% in ^{175}Lu. Absolute abundances were fixed by normalising ^{42}Ca to the CaO concentration determined by EPMA; total ^{42}Ca was chosen to counteract the effect of including some host olivine in the analysis of some smaller melt inclusions. Oxide interferences were corrected for, with minor adjustment being made using BCR-2G. A matrix correction was applied using measurements of GSD-1G, BCR-2G, BHVO-2G, BIR-1G, GOR132-G and ML3B-G, where a correction factor was calculated for each element using a linear regression through all standards (published values from GeoReM, Jochum et al., 2005). The maximum correction was +25% for Rb. Precision was calculated using repeat analyses of some standards, with relative $1\sigma = 1$–12% for the elements analysed (see Supplementary Tables A2 and A3). Trace element data were collected by SIMS from 69 picrite inclusions and 85 ferropicrite inclusions.

4. COMPOSITIONS OF OLIVINE-HOSTED MELT INCLUSIONS

Major and trace element analyses of 154 olivine-hosted melt inclusions and the corresponding whole-rock data are given in Supplementary Tables A1 and A4, respectively. Our discussion of melt inclusions from the Etendeka picrites is supplemented by 31 major element analyses and 16 trace element analyses of picrite melt inclusions by Keiding et al. (2011; sample JVT-09–32 from that study was excluded due to its erratic melt inclusion compositions).

4.1. Major elements

Comparisons between the concentrations of major elements in olivine-hosted melt inclusions and their corresponding whole-rocks are shown in Fig. 4. These plots reveal that for both the ferropicrites and picrites the compositional trends of the melt inclusions and associated whole-rocks are fairly dissimilar. Certain features of the whole-rock data are broadly mirrored by the inclusions: for example, the Dronning Maud Land ferropicrites are lower in Al_2O_3 and Na_2O than the Etendeka ferropicrites at a given Fo content (Fig. 4a, e, f and j). However, for most major elements the trends in the melt inclusion compositions do not clearly correspond to the whole-rock data (which in some cases are affected by crystal accumulation). The melt inclusions do not easily define a liquid line of descent, i.e. inclusions within a given sample group (Etendeka picrites; Etendeka ferropicrites; Dronning Maud Land ferropicrites) are not related through fractional crystallisation alone. This can be seen, for example, in the counterintuitive decrease in Na_2O with increasing degree of crystallisation (decreasing Fo) in the Etendeka ferropicrite samples, and the steeper than expected increase in FeO_T with crystallisation. Melt inclusions that are hosted by olivines with the lowest Fo contents in the Etendeka ferropicrites (97SB67 and 97SB68; $Fo_{63–73}$) reach extremely high FeO_T concentrations (up to 32 wt.%; Fig. 4b), which is more than double the FeO_T content (13.7 wt.%) of the associated whole-rock (Fig. 4g). Moreover, Fig. 4 shows that the melt inclusions exhibit a high degree of variation of all elements at a given Fo content. These characteristics, especially in the lowest Fo samples, are not explained by fractional crystallisation and the relationship between the major-element chemistry of the melt inclusions and host olivine Fo is striking. We examine the origins of these relationships in Section 5.1.1.

4.2. Trace elements

Primitive-mantle normalised incompatible trace element plots (Figs. 5 and 6) show that, amongst both picrite and ferropicrite magma types, the compositions of most melt inclusions are approximately equivalent to their respective whole-rock compositions, and their average concentrations tend to converge on the whole-rock composition. Some melt inclusions have elevated concentrations of Rb, Ba, K and/or Sr. Excluding these inclusions, all samples have melt inclusion populations with rather uniform trace element ratios. Those in the ferropicrites (except for sample 97SB67, which has low Fo olivine and low initial ε_{Nd} of −2.9) are extremely similar and near-identical to the whole-rock.

Shifts in normalised patterns of melt inclusion concentrations to higher or lower values relative to whole-rock patterns can occur as a consequence of olivine loss or gain. During re-homogenisation, variable amounts of remelted olivine from the melt inclusion rim act to dilute or concentrate all incompatible elements, which shifts incompatible elements in melt inclusions relative to the parental liquid. It is likely that the majority of inclusions in this study are under-heated (see Section 5.1.1) and so incompatible trace elements are concentrated relative to parental liquid values. In addition, accumulation or loss of olivine phenocrysts shifts whole-rock compositions relative to the initial liquid. Nevertheless, assuming that all of the analysed trace elements are fully incompatible in olivine, these effects should not modify their relative concentrations, and patterns on a normalised multi-element plot should remain parallel. For this reason, trace element ratios are preferred to absolute concentrations when interpreting re-homogenised melt inclusion data.

Incompatible trace element ratios of the olivine-hosted melt inclusions are plotted in Fig. 7 and indicate that the Etendeka and Vestfjella ferropicrites are more enriched in the highly incompatible elements than the Etendeka picrites and Ahlmannryggen ferropicrites. Almost all of the Etendeka and Vestfjella ferropicrite melt inclusions, however, have higher LREE/HREE (La/Yb) and MREE/HREE (Sm/Yb) ratios (Fig. 7a and c) than those from picrites, with the offset especially apparent at high host olivine Fo content. The Ahlmannryggen ferropicrite inclusions also have higher MREE/HREE ratios than the picrites. There

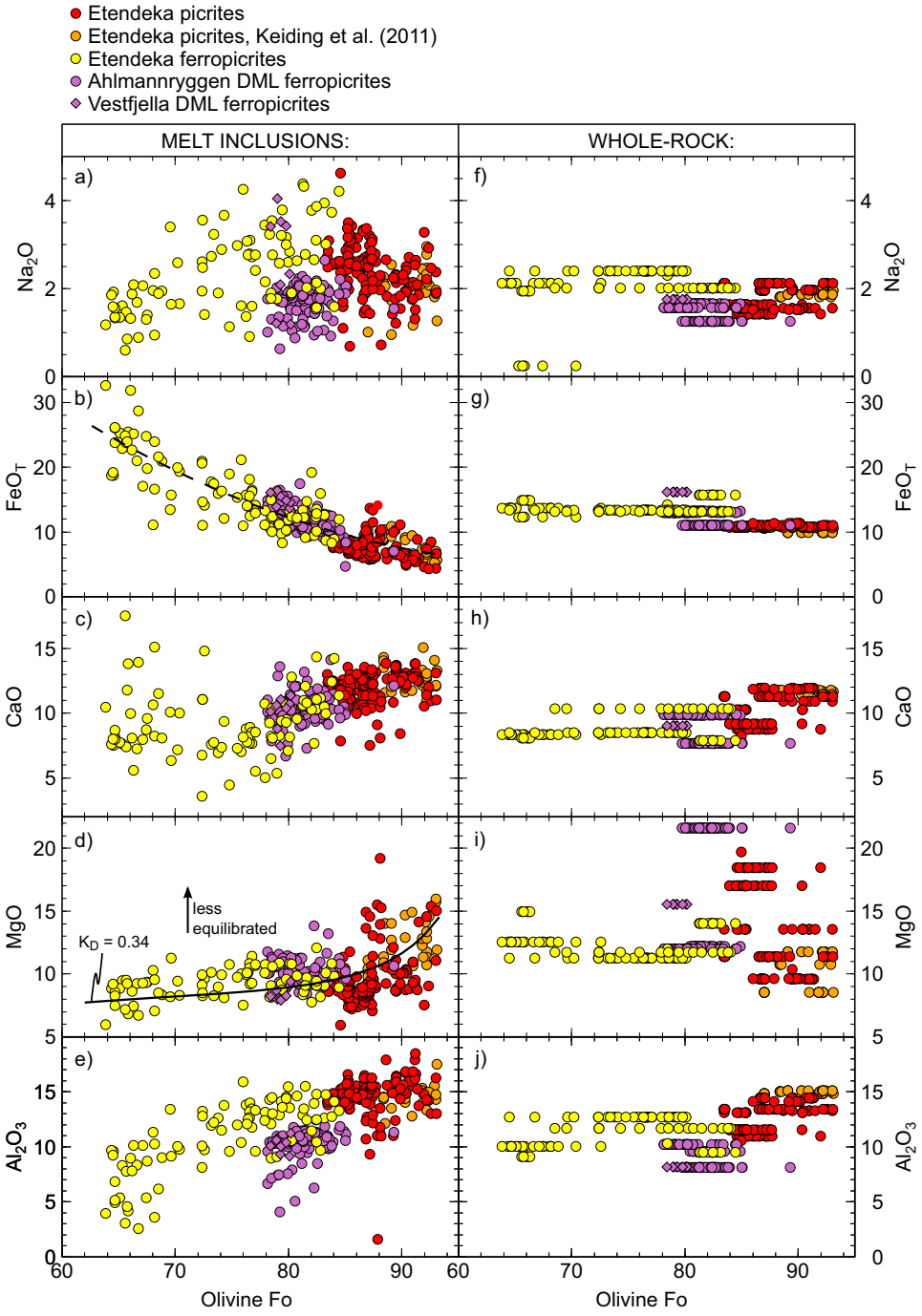

Fig. 4. Major element compositions (wt.% oxides) of re-homogenised melt inclusions, not corrected for post-entrapment crystallisation, plotted against host olivine forsterite content (a–e). In plots f–j, the Fo content of the same olivine hosts as in a–e are shown on the *x*-axis, plotted with their respective bulk rock composition (Gibson et al., 2000; Thompson et al., 2001; Riley et al., 2005; Heinonen et al., 2010; Keiding et al., 2011) on the *y*-axis. Legend at top of figure. (b) The dashed line is a polynomial regression through all the data. (d) The solid line is calculated MgO content in equilibrium with the relevant Fo and FeO_T from the regression of (b), using $K_D^{Fe-Mg} = 0.34$ (Matzen et al., 2011) and $Fe^{3+}/\Sigma Fe = 0.05$ (appropriate for FMQ-1 and 1200 °C furnace conditions; Kress and Carmichael, 1991). Less equilibrated inclusions would have higher MgO.

is a strong contrast in the Sc/Zr ratio (Fig. 7d) between the high-Fo ferropicrites and picrites. Finally, the very tight distribution of ratios of incompatible trace elements on Fig. 7 shows that there is little variability between melt inclusions, particularly within the Etendeka picrites and Ahlmannryggen ferropicrites.

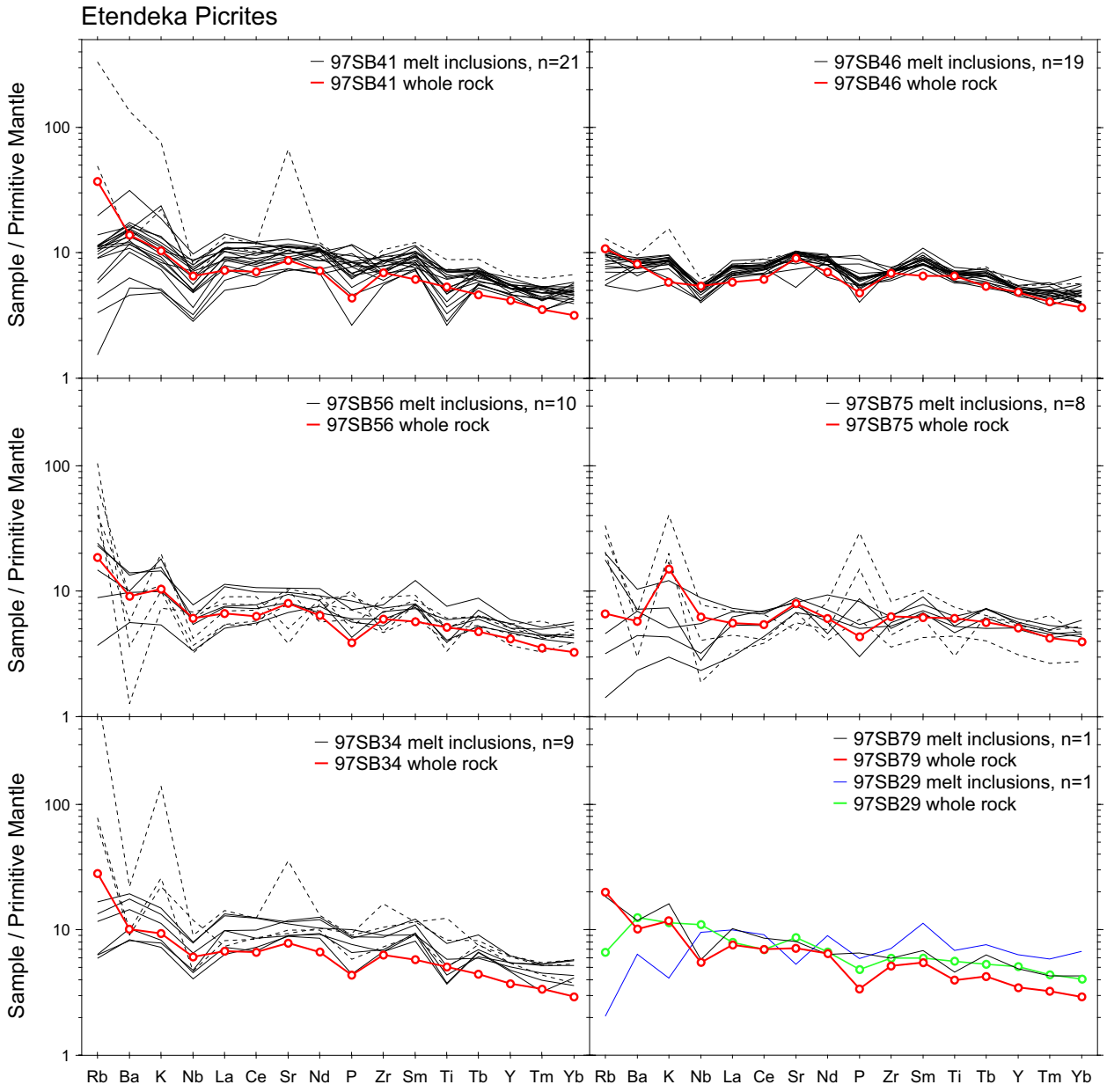

Fig. 5. Primitive mantle (McDonough and Sun, 1995) normalised multi-element plots showing selected REE and other trace element concentrations in the Etendeka picrites, measured by SIMS, except P, which was measured by EPMA. Solid black lines, melt inclusions; dotted black lines, melt inclusions interpreted as altered; thick red or green lines with open symbols, published whole-rock ICP-MS composition. Each plot represents one or two whole-rock samples. (For interpretation of the references to colour in this figure legend, the reader is referred to the web version of this article.)

5. DISCUSSION

5.1. The compositions of the melt inclusions: mantle source, crustal processing and rehomogenisation

5.1.1. The major element compositions of rehomogenised melt inclusions

The major element contents of the melt inclusions (Fig. 4) are difficult to relate to the whole-rock compositions and do not define a clear crystallisation trend, with the extremely high FeO_T contents at low Fo being of particular interest (Fig. 4b). Such high FeO_T contents in the melt inclusions cannot represent any primary or subsequently fractionated composition derived by partial melting of mantle peridotite or pyroxenite (e.g. Kogiso et al., 1998; Herzberg and O'Hara, 2002). In addition, FeO_T forms a smooth and relatively low-scatter trend with Fo that is continuous across the different sample types. This intriguing trend is in contrast with that expected from the whole-rock data, given that the distinction between picrite and ferropicrite is made by a marked difference in their FeO_T content.

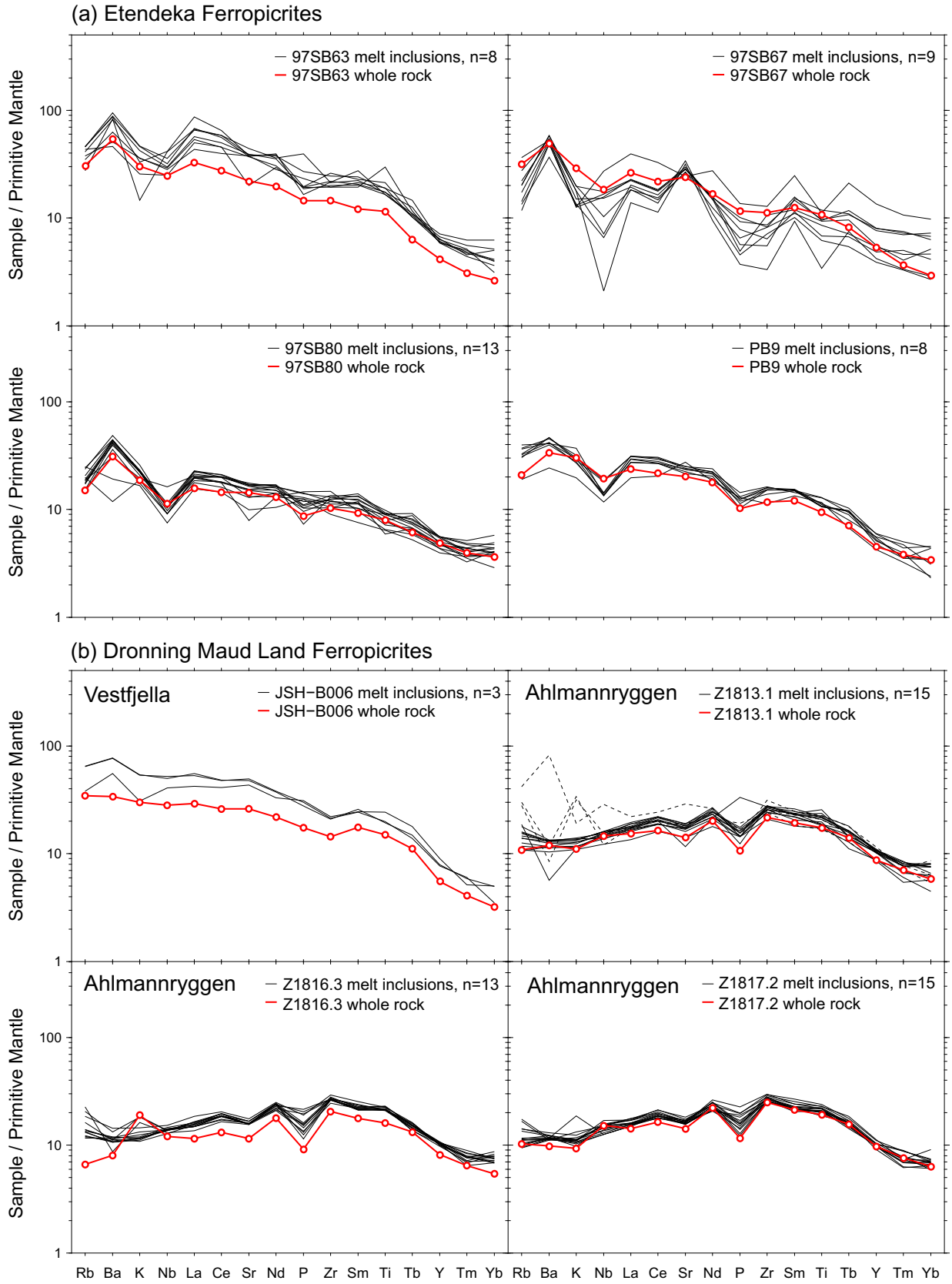

Fig. 6. Primitive mantle (McDonough and Sun, 1995) normalised multi-element plots showing selected REE and other trace element concentrations in (a) the Etendeka ferropicrites and (b) Dronning Maud Land (Ahlmannryggen and Vestfjella); details as for Fig. 5.

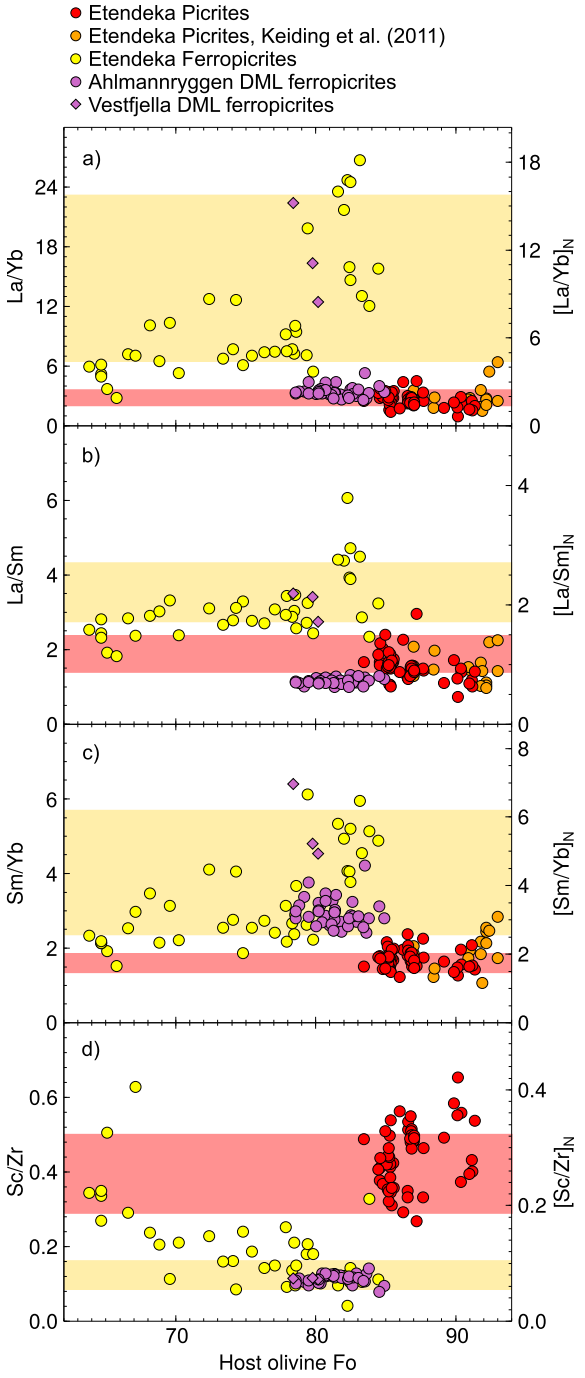

Fig. 7. Trace element ratios of homogenised melt inclusions (excluding those identified as altered in Figs. 5 and 6) plotted against host olivine Fo content. Shaded pale red field shows the picrite whole-rock range and shaded yellow field shows the Etendeka ferropicrite whole-rock range. Right-hand axes show primitive-mantle normalised ratios (McDonough and Sun, 1995). (For interpretation of the references to colour in this figure legend, the reader is referred to the web version of this article.)

We suggest that the major element compositions of these melt inclusions have been significantly modified by post-entrapment crystallisation and re-homogenisation. Post-entrapment crystallisation causes successively more fayalite-rich layers of olivine from the trapped melt inclusion to precipitate on the host crystal wall. These layers quickly re-equilibrate with the surrounding olivine crystal and effectively vanish, causing an apparent 'Fe-loss' in the inclusion (Danyushevsky et al., 2000). During re-homogenisation in a furnace, some unknown amount of wall olivine remelts. Insufficient olivine will remelt if the temperature is too low, whereas if the temperature is too high, excess olivine will be added to the melt. In this case, the excess heating results in the opposite effect of the 'Fe-loss' process described by Danyushevsky et al. (2000). This involves: (i) addition of excess MgO *and* FeO from the relatively Fe-rich olivine to the melt inclusion by olivine melting, then (ii) re-equilibration of the melt with the surrounding olivine to maintain the correct K_D^{Fe-Mg} via exchange of Fe^{2+} cations in the crystal with Mg^{2+} cations from the melt. This process, also predicted to occur by Danyushevsky et al. (2000), relies on adequate diffusion occurring over the heating period of 20 min in this study. When re-equilibration occurs, the apparent K_D^{Fe-Mg} can no longer be used to correct the inclusion composition, as is commonly done for cases of post-entrapment crystallisation (e.g. Gurenko and Chaussidon, 1995; Danyushevsky et al., 2000; Danyushevsky and Plechov, 2011).

In our study, the majority of the inclusions are underheated, as they were judged to be homogeneous once all daughter phases except for olivine had disappeared. This process has concentrated elements that are incompatible in olivine in the melt inclusions so that their concentrations are slightly high relative to the associated whole-rock (Figs. 5 and 6). The lowest Fo samples (97SB67 and 97SB68) were likely overheated because the opaque veneer on the crystals together with their dark melt colour and low frequency of inclusions made it difficult to visually assess the homogenisation temperature. It is expected that, within a given sample, low Fo olivines would be more overheated than high Fo olivines because they originally crystallised at lower temperature. The addition of excess olivine results in a dilution trend which lowers the concentration of all the other major elements and may account for some of the major element trends observed in Fig. 4. For example, the positive correlation of Na_2O and Al_2O_3 with Fo in Etendeka ferropicrites could be explained by dilution, although dilution fails to explain the high and scattered CaO in some low Fo ferropicrite olivines.

The trend whereby low-Fo inclusions are enriched in FeO_T (Fig. 4b) can be explained by re-homogenisation if the melt inclusions approximately maintained equilibrium with their host. The feasibility of this process is supported by the relationship between Fo, FeO and MgO in our data. The dashed line given on Fig. 4b is a polynomial regression through all the melt inclusion FeO_T contents (the purpose of this is to test for Fe-Mg equilibrium – it is not a liquid line of descent and does not imply that the sample groups are linked). The solid line shown in Fig. 4d shows the calculated melt MgO content of inclusions in equilibrium with the regression line of Fig. 4b (assuming $K_D^{Fe-Mg} = 0.34$; Matzen et al., 2011, and $Fe^{3+}/\Sigma Fe = 0.05$ at furnace conditions; Kress and Carmichael, 1991) and the host olivine. The inclusions generally follow the trend shown by this line,

indicating that olivine and melt inclusions are in approximate equilibrium. This suggests that the surprisingly high FeO_T contents of inclusions hosted in low-Fo olivine are simply a function of their MgO content and host olivine Fo. Thus, the high FeO_T content of these inclusions does not require a special explanation. Unfortunately, the extent to which excess olivine was added is not known because the pre-homogenisation inclusion compositions are not known. As an example, an initially 13 wt.% FeO, 8.4 wt.% MgO inclusion hosted in Fo_{66} olivine would become 24 wt.% FeO and 9.5% MgO following the consumption of 25% host olivine and full re-equilibration. Partial re-equilibration would result in inclusions having a higher MgO content (marked on Fig. 4d) and lower FeO content at a given Fo, i.e. an intermediate composition in the given example. The suggestion that this mechanism is occurring in all inclusions from all sample groups is additionally supported by the smooth trend in FeO_T with Fo content regardless of group (Fig. 4b), and by the observation of a narrow (~5 μm) high-Fo rim around re-heated melt inclusions and a broader low-Fo rim around non–heated inclusions. Gaetani and Watson (2000) observed that excess heating results in an increase in both the MgO and FeO_T contents in high Fo olivine-hosted inclusions. It should be noted that this process will not affect the host olivine Fo beyond the immediate inclusion rim.

An alternative explanation could be that, for the olivines with relatively low Fo, the high FeO_T results from the resorption of magnetite. Excess magnetite could be caught in heterogeneous trapping, or could have formed within melt inclusions after entrapment as a response to H^+ diffusion out through the olivine during initial cooling (Rowe, 2006). The magnetite would have melted during high temperature re-homogenisation, resulting in excess Fe entering the melt. However, although some crystalline (unhomogenised) inclusions in low Fo olivine contain large magnetite crystals, most do not, so trapped magnetite cannot explain the observed systematic trend.

Across all sample types, FeO_T in olivine-hosted melt inclusions, but not their host rocks, varies smoothly with host olivine Fo content (Fig. 4b and g). This effect is an artefact and serves as a warning that re-homogenised melt inclusions are not reliable indicators of the original melt Fe/Mg, and thus are unsuitable material for the application of Fe-Mg based thermometers (cf. Keiding et al., 2011).

5.1.2. Anomalous melt inclusion trace element compositions: Hydrothermal alteration and/or crustal assimilation?

Isotopic evidence rules out a significant contribution from the metasomatised subcontinental lithospheric mantle (SCLM) to the picrites and ferropicrites (Gibson et al., 2000; Thompson et al., 2001; Heinonen et al., 2010, 2014). The peaks and troughs at Rb, Ba, K and/or Sr on normalised multi-element plots displayed by some olivine-hosted melt inclusions (Figs. 5 and 6) are not expected to be a feature of their mantle source, and show that their initial melt compositions have been modified. They could instead be due to either crustal assimilation (pre-entrapment) or hydrothermal alteration (post-entrapment). These melt inclusions do not have particularly elevated levels of other highly incompatible elements (such as La), which typically occur in higher concentrations in continental crust, suggesting that they may instead have undergone alteration by a hydrous fluid.

Whether the inclusions also represent the effects of crustal assimilation can be further interrogated by examining the relationship between the extent of crystallisation and trace element ratios that are sensitive to both contamination and hydrothermal alteration. In this case, we examine Rb/Zr in Etendeka samples and Ba/Zr in Karoo samples, as these element combinations should give a strong signal from the respective assumed contaminants. We follow Thompson et al. (2007) and assume that the upper crust local to the Etendeka is represented by a Damara Belt granite (VB12), and use its composition to assess the effects of crustal assimilation on these magmas. The incompatible trace element compositions of some other potential contaminant reservoirs for the Etendeka samples are shown in Fig. 9. Ferropicrites in Dronning Maud Land were probably emplaced through a predominantly Tonalite–Trondhjemite–Granodiorite (TTG) basement, here represented by an average TTG composition from the Kaapvaal Craton (Kreissig et al., 2000), which is contemporaneous with the Grunehogna craton where Ahlmannryggen is situated (Marschall et al., 2010). If a cooling magma melts and assimilates wallrock material, it is expected that melt inclusions trapped after extensive crystallisation (i.e. hosted in low-Fo olivine) will be more contaminated than inclusions in earlier olivine crystals (DePaolo, 1981), so sensitive trace element ratios should correlate with Fo. Melt inclusion compositions are plotted as a function of Fo in Fig. 8. Only a small subset of inclusions has highly elevated Rb/Zr or Ba/Zr; these do not correlate with the host olivine Fo and are seemingly random. For comparison, two lines are shown on each plot of Fig. 8. One shows the modelled trace element ratio evolution of a magma experiencing only fractional crystallisation – it is essentially flat and describes most of the data. The other indicates the trace element evolution trend that could be expected if the magma were to simultaneously assimilate crustal material and fractionate crystals in a fixed 1:1 weight ratio. The melt inclusion compositions do not follow a curve at all, let alone one with a shape like that shown, from which it can be concluded that the magma from which they were trapped did not experienced systematic or significant crustal assimilation.

Rb and Ba are sensitive to hydrothermal alteration as well as crustal assimilation, and we note that the inclusions with elevated Rb/Zr or Ba/Zr also have anomalous peaks or troughs in K and Sr concentrations (Figs. 5 and 6). Given that these elements are all fluid-mobile, the trace element compositions of the anomalous inclusions are best explained by hydrothermal alteration. This is consistent with petrographic evidence from thin sections which shows that around half of all inclusions are breached, as well as evidence for hydrothermal alteration in some whole-rock samples (serpentinisation and groundmass chlorite). However, the possibility of wallrock assimilation cannot be ruled out and could have sporadically affected individual inclusions; a localised wallrock reaction instead of gradual assimilation would negate the requirement for assimilation to be systematic (Danyushevsky et al., 2004).

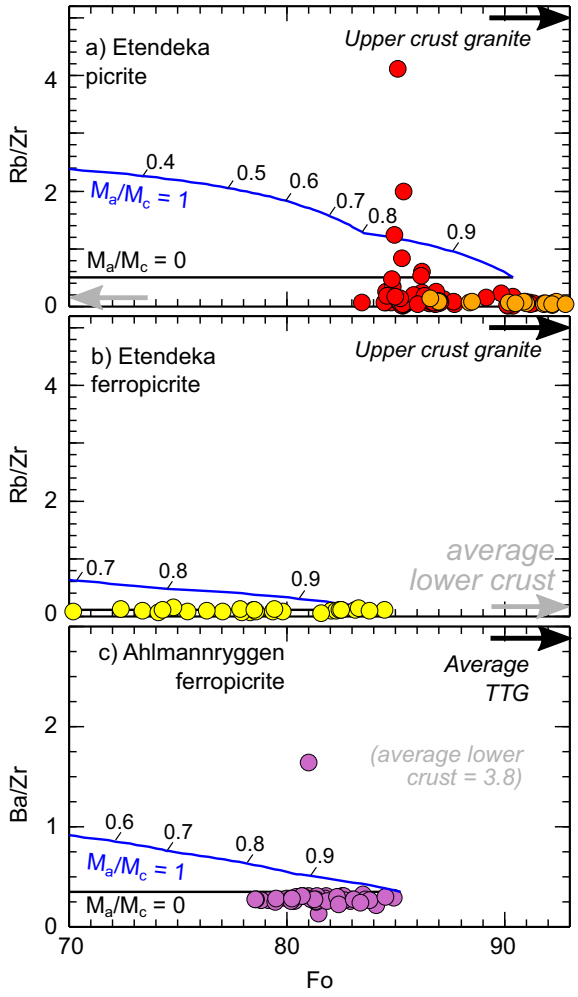

Fig. 8. Melt inclusion Rb/Zr or Ba/Zr ratio as a function of host olivine Fo (filled circles). Black curves show the melt compositional trend expected in the case of fractional crystallisation alone ($M_a/M_c = 0$), modelled in Petrolog3 (Danyushevsky and Plechov, 2011). Details of the models and symbols are as follows: (a) Etendeka ferropicrites (model from 97SB63 whole-rock composition, QFM, 5 kbar); (b) Etendeka picrite samples (this study in red; Keiding et al., 2011 in orange, model is 97SB33 whole-rock composition corrected for olivine accumulation, QFM, 3 kbar); (c) Ba/Zr ratio, Dronning Maud Land ferropicrites (model is Z1813.1, QFM, 5 kbar). Model melt compositions are plotted against equilibrium Fo. The blue curves, marked at $F = 0.1$ intervals, indicate the expected trend if fractionation and accumulation occurred at equal mass ratio ($M_a/M_c = 1$), calculated using the pure fractionation trend and assimilant composition. This should not be treated as a rigorous predictive model, rather a rough guideline for the shape of trends expected if the melt was systematically assimilating crustal material. Assimilant compositions indicated by arrows: Etendeka upper crustal granite, sample VB12 (Thompson et al., 2007); average TTG is average of samples from Kreissig et al. (2000). Also shown with a grey arrow is the average lower crustal composition of Rudnick and Fountain (1995). (For interpretation of the references to colour in this figure legend, the reader is referred to the web version of this article.)

The remaining unaltered inclusions do not show evidence for the systematic assimilation of wallrock material. This is consistent with the low levels of contamination observed in the whole-rock samples on the basis of isotopic evidence (Gibson et al., 2000; Thompson et al., 2001; Heinonen et al., 2010, 2014). The olivine-hosted melt inclusions in the picrites and ferropicrites included in this study actually appear less contaminated than the host whole-rock samples (cf. melt inclusions from the Yemen CFB province, Kent et al., 2002). The fact that Rb/Zr and Ba/Zr do not resolvably increase with the degree of crystallisation can be described in terms of a mass ratio of assimilated to crystallised material (M_a/M_c) of <0.1 over this crystallisation interval; assigning such a value allows comparison of these inclusions with those from other CFB provinces. A maximum of 0.1 is slightly lower than in the North Atlantic Igneous Province (Mull = 0.1–0.3; Peate et al., 2012), and much lower than the extremely contaminated inclusions found in primitive melts from Yemen (1–10; Kent et al., 2002). Importantly, the melt inclusions in the present study have preserved their trace element characteristics from their origin as mantle melts, with any alteration process being difficult to detect (except in the subset of inclusions identified in Figs. 5 and 6). This allows the inclusion compositions to be interpreted in the context of mantle processes.

5.1.3. The trace element compositions of melt inclusions and their mantle source

The offset in $[LREE/HREE]_N$, $[MREE/HREE]_N$ and Sc/Zr between picrites and ferropicrites (Fig. 7) point towards mineralogical differences in their respective mantle source lithologies. A higher $[MREE/HREE]_N$ indicates the increased importance of residual garnet within the ferropicrite mantle source (e.g. Gibson et al., 2000), which may be caused by the involvement of a more enriched lithology and/or increased melting pressure. Sc is moderately compatible in both clinopyroxene and garnet (e.g. Tuff and Gibson, 2007), so the lower Sc/Zr in ferropicrites may reflect an elevated clinopyroxene and garnet content in the ferropicrite source, i.e. garnet clinopyroxenite rather than peridotite (Gibson, 2002; Tuff et al., 2005). The alternative explanation that clinopyroxene crystallisation reduced the melt Sc/Zr is probably not correct as no correlation is seen between this ratio and Fo in samples with Fo > 70. These ratios are not fractionated by olivine crystallisation or post-entrapment processes, so preserve the composition of the parental trapped melts and reflect mantle melting conditions.

We note that the melt inclusion trace element compositions are very similar to their host bulk-rock composition, despite the fact that the host rock has not been encapsulated and preserved in the same way as the (unbreached) inclusions have. This implies that whole-rock analyses of similar hand specimens from other old provinces can still provide a meaningful approximation of their initial liquid chemistry.

5.2. Primary variability in incompatible trace elements of olivine-hosted melt inclusions

5.2.1. Origin of the (limited) melt inclusion variability in primitive Paraná–Etendeka and Karoo CFB rocks

The variability in incompatible trace element contents of olivine-hosted melt inclusions in primitive magmas from

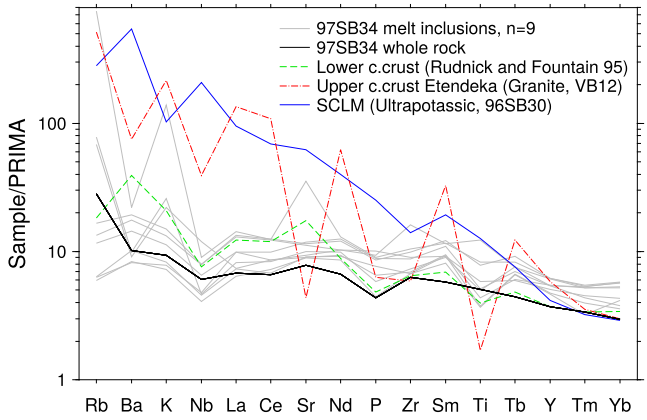

Fig. 9. Multi-element plot of potential Etendeka contaminants normalised to primitive mantle (McDonough and Sun, 1995). Trace elements from melt inclusions (grey lines) and whole-rock (black line) are provided for an Etendeka picrite (97SB34). Shown for comparison are the composition of upper crust (Granite, VB12; Thompson et al., 2007) and subcontinental lithospheric mantle melt (SCLM, Lamprophyre, 96SB30, Thompson et al., 2001) local to the Etendeka province and estimated lower crustal composition of Rudnick and Fountain (1995). (For interpretation of the references to colour in this figure legend, the reader is referred to the web version of this article.)

the Paraná–Etendeka and Karoo CFBs is low, and most inclusion compositions are similar to the respective whole-rock composition. Nevertheless, the level of variability observed in the uncontaminated inclusions is statistically meaningful and above analytical uncertainty on the basis of signal-to-noise ratio (S/N), at the 99% confidence level for picrites ($n = 71$, $S/N = 2.2$) and 95% for the ferropicrites ($n = 72$, $S/N = 1.3$). Its origin is examined through principal component analysis (PCA), as has been previously done to interpret melt inclusion variability (e.g. Slater et al., 2001; Maclennan et al., 2003). A detailed description of the purpose and results of PCA analysis can be found in the supplementary material, and the findings are summarised here. The greatest source of variability seen in all samples (PC1) is attributed to the dilution effect of adding or subtracting varying proportions of olivine to the melt, which affects trace element concentrations but not their relative proportions. A number of processes could generate the PC1 signal, including post-entrapment crystallisation, experimental re-homogenisation of the inclusions, and variable amounts of olivine fractionation. PC2 is characterised by anti-correlation of the highly incompatible trace elements and HREE + Y in the melt inclusions, which is likely to be the result of varying strengths of a garnet signature – a mantle signal. It may result from variations in lithology and/or depth of melting and segregation of instantaneous fractional melts. In general, the low level of variability in the inclusions means that these two components do not account for all of the variability (only 48–80%), though much of the remaining signal may be analytical noise.

5.2.2. Comparison of melt inclusion variability with global LIP, MORB and OIB datasets

The level of trace element variability observed in melt inclusions analysed in this study is compared with datasets of global MORB, OIB and Large Igneous Provinces (LIP) in Fig. 10. The datasets are filtered to remove: highly contaminated inclusions (see caption to Fig. 10); $Fo_{<82}$ inclusions in basalts and picrites; and $Fo_{<76}$ inclusions in ferropicrites. The samples are from individual hand specimens, usually from different lava flows and dykes, but occasionally from the same flow. The ratios and concentrations shown in Fig. 10 are moderately insensitive to crystallisation and hydrothermal alteration, and were selected to examine variability originating in the mantle source and melting process. Note that Iceland is treated as a separate category to MAR and OIB in this analysis, and that CFB provinces and the Ontong Java Plateau (OJP) are jointly considered as LIP. The number of whole-rock samples in the global dataset that passed the criteria for inclusion is relatively small ($n = 63$–69, depending on the element) and over a third of the samples are from Hawaii.

The compositional variability of olivine-hosted melt inclusions tends to be highest in samples from the Mid Atlantic Ridge (MAR) and Iceland and lowest in the ferropicrites (Fig. 10). In all groups the range in standard deviations is large, showing that the degree of variability is not consistent between whole-rock samples. Globally, there appears to be a tectonic setting control: in terms of La/Y and La, the mean variability of each group is ranked as MAR > plume-affected ridge (Iceland) > OIB and LIP > ferropicrite, whereas in terms of Ti/Zr and Sm/Zr, it is Iceland > MAR > OIB and LIP > ferropicrite. Melt inclusions from global ocean islands and LIPs have a similar low level of variability to those from the Paraná–Etendeka province analysed in this study. Peate et al. (2012) also noted that melt inclusions from the North Atlantic Igneous Province (Mull) were rather homogeneous in trace elements that are insensitive to contamination. There are, of course, individual samples and locations that go against the general trend, for instance the OJP inclusions are more variable than the LIP average, and one Etendeka ferropicrite sample is as variable as the LIP average. Variability in melt inclusions from Yemen (Kent et al., 2002) is slightly higher than for other CFB provinces, which reflects the fact that the Yemen dataset contains many melt inclusions that suffered levels of assimilation high enough to introduce variability, but low enough that not all are

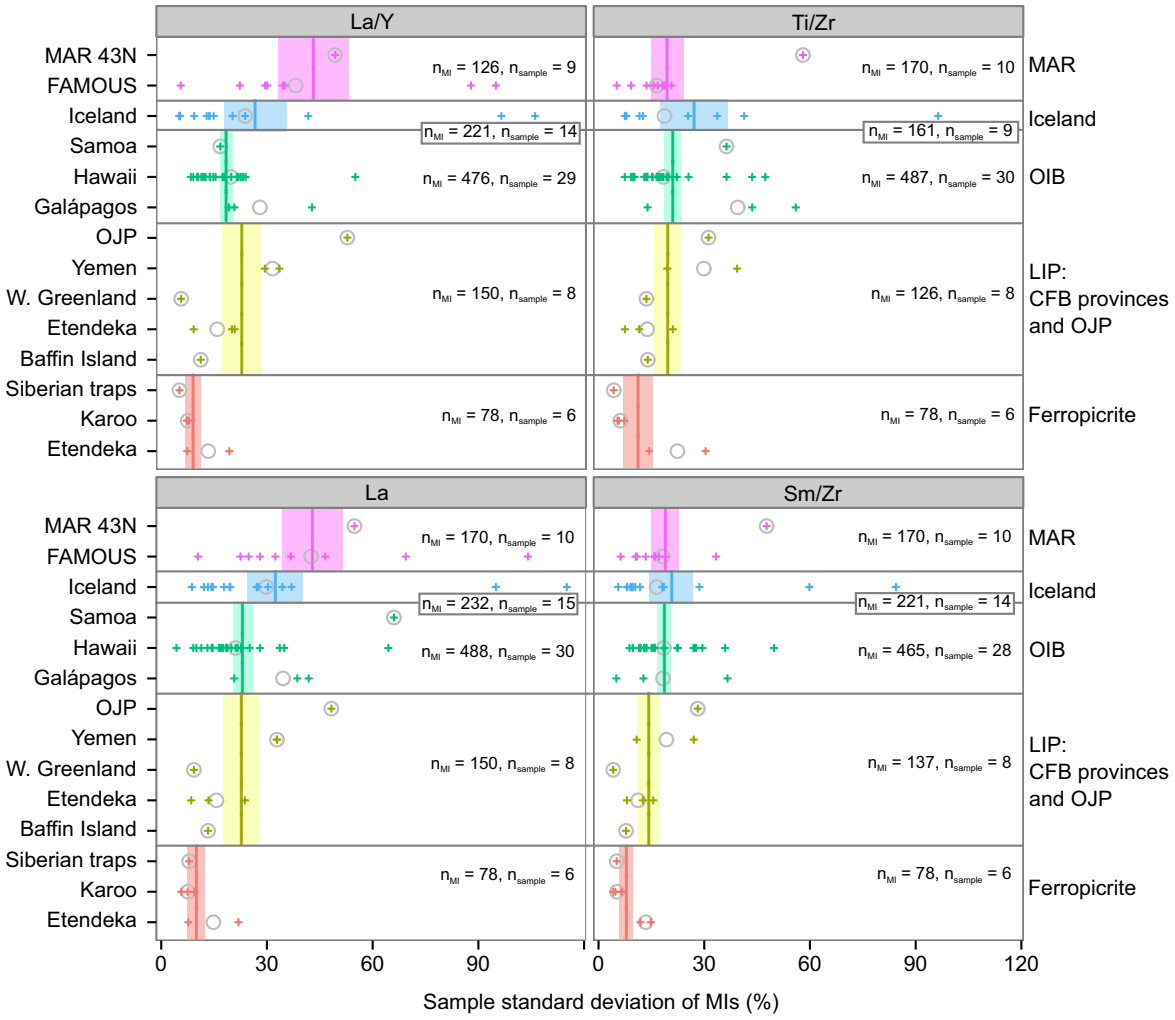

Fig. 10. La/Y, La, Ti/Zr and Sm/Zr variability in melt inclusions from global datasets of MORB, OIB and CFB provinces. Arbitrary filters are applied to remove altered inclusions (Rb/Zr > 0.25 or Ba/Zr > 3 or K_2O > 2.0 wt.%, depending on which elements are provided), evolved inclusions (Fo < 82, basalts and picrites; Fo < 76, ferropicrites), and samples with fewer than 8 inclusions after those filters are applied. Points (+) represent the standard deviation of melt inclusions in a single sample or lava flow expressed as a percentage of the mean, such that all samples are directly comparable; circles represent the weighted mean standard deviation of all samples for a given location; vertical lines represent the mean standard deviation of samples for a given grouping. Rectangle is the standard error of the mean. Data sources are as follows: FAMOUS, Laubier et al. (2012), Shimizu (1998); 43°N MAR, Kamenetsky et al. (1998); Iceland, compilation of Maclennan (2008a), Neave et al. (2013, 2014); Hawaii, Norman et al. (2002), Sobolev et al. (2011) and Sides et al. (2014); Galápagos, Koleszar et al. (2009); Ontong Java Plateau (OJP), Jackson et al. (2015); Baffin Island, Starkey et al. (2012); West Greenland, Starkey et al. (2012); Yemen, Kent et al. (2002); Siberian Traps ferropicrites, Sobolev et al. (2009), Gudchikhinsky fm. samples from Noril'sk, identified as ferropicrite by Gibson, 2002); Paraná-Etendeka and Karoo CFB provinces, this study and Keiding et al. (2011).

effectively removed during data filtering. Olivine-hosted melt inclusions from CFB ferropicrites are always the least compositionally heterogeneous group.

To put the degree of heterogeneity observed in Fig. 10 into context, it is useful to consider the maximum variability expected in incremental fractional mantle melts. For this purpose, La concentrations are used. By assuming a one dimensional melting column and a mantle source composition (C_0), and given that the partition coefficient of La (D_{La}) $\ll 1$, the fraction of melting (F) required to match the aggregated mantle melt composition (C_l; this is taken as the mean melt inclusion La concentration of a given sample type) can be calculated using the approximate relationship $F \approx C_0/C_l$ (Table 1). Assuming perfect fractional modal melting, equation D.6 of Rudge et al. (2013) can then be used to predict the variance of incremental melts:

$$\sigma_0^2 = \frac{C_0^2}{2FD}.$$

Where D is the bulk solid-melt partition coefficient. The results of this calculation are given in Table 1, and details of the values used are given in the caption. Observed (σ) and predicted (σ_0) standard deviation are presented as a percentage of the relevant mean melt inclusion concentration, which is also used to calculate F. σ_0 ranges from 140% to 234%, which is much higher than the observed

Table 1
Degree of mixing (M) calculated for different tectonic settings and magma types using La concentration of olivine-hosted melt inclusions.

	MI mean La, ppm, observed	MI σ, %, observed	C_0, ppm	F	D	Model σ_0, %	M (±)*	n_{MI} (n_{sample})
MAR	2.9	42.9	0.23	0.082	0.012	187	0.947 (0.006)	171 (10)
Iceland	5.0	32.9	0.65	0.129	0.012	234	0.980 (0.002)	239 (15)
OIB	12.5	23.1	0.65	0.052	0.012	149	0.976 (0.003)	488 (30)
CFB province	6.4	21.7	0.65	0.101	0.012	208	0.989 (0.001)	140 (8)
Ferropicrite	14.1	10.0	1.16	0.083	0.021	140	0.995 (0.005)	78 (6)

MI mean and σ are the calculated mean and standard deviation of the La contents of melt inclusions in the global dataset considered in this study (host Fo > 82 only, or Fo > 76 for ferropicrite). C_0 is the assigned initial source composition: the concentration of La in the primitive mantle of McDonough and Sun (1995) is used, except in the case of the Mid Atlantic Ridge (MAR), for which the depleted mantle concentration of Salters and Stracke (2004) is used, and for ferropicrite, where a 1:1 mixture of primitive mantle and subduction-modified igneous crust (Stracke et al., 2003a) is used. Melt fractions (F) are calculated from melt inclusion mean value. The bulk solid-melt partition coefficient (D) is calculated using the mineral-melt partition coefficients of Gibson and Geist (2010) and the 30 kbar peridotite solidus phase proportions of Davis et al. (2011), except in the case of ferropicrite, where the preferred eclogite value from Pertermann et al. (2004) is used. M is the mixing parameter, where $M = 1$ is completely homogeneous and $M = 0$ refers to fully unmixed incremental mantle melts. n is the number of melt inclusion analyses considered, with the number in brackets indicating the corresponding number of samples.

* Uncertainty in M is illustrative of the effect of uncertainty in C_0 of 10%, or 50% in the case of ferropicrite.

values; for example, the observed La variability on Iceland is 33%, which is a large reduction from the 234% predicted for incremental fractional mantle melts, and reflects extensive mixing after melt formation. The extent to which these incremental melts would have had to mix (M) in order to reduce their variability down to that recorded in melt inclusions can be calculated using the equation of Maclennan (2008a):

$$M = 1 - \left(\frac{\sigma^2}{\sigma_0^2}\right).$$

It should be noted that each melt type was assumed to come from a homogeneous source (peridotite or pyroxenite). Because contributions from both source types could exist in the accumulated melts the predicted σ_0, and thus M, is a minimum value. In addition, the calculated M is sensitive to C_0 in depleted compositions. An uncertainty in M is provided in Table 1 to illustrate the effect of a 10% uncertainty in source composition (except for ferropicrite, for which a 50% uncertainty is used, given the lack of consensus on the composition of mantle pyroxenite).

Table 1 shows that in all cases M is > 0.95, so the vast majority of mixing occurred prior to the onset of crystallisation and melt inclusion entrapment in all settings. In terms of La concentration alone, the order in which the groups show increasing mixing extent M is approximately the same as that indicated in Fig. 10: MAR < Iceland and OIB < LIP < ferropicrite. Ferropicrites are the most extensively mixed with $M > 0.99$, so despite their origin in a necessarily heterogeneous mantle source, the melt inclusions indicate that the instantaneous melts homogenised quickly with respect to the onset of crystallisation. Some caveats apply to these calculations: they rely on a heavily simplified melt model and assume that instantaneous fractional melts are isolated from the moment of their formation, which may overestimate the expected variability of the flux of melt from the mantle melting region. Melt inclusions from all CFB provinces are re-homogenised and some variability in La concentrations may be due to the dilution effect. Nevertheless, our calculation suggests that all primitive magmas have been significantly mixed since their formation in the mantle, and CFB and ferropicrite magmas especially so.

5.2.3. Comparison between the relative timing of mixing and crystallisation processes in CFB provinces and Iceland

Melt inclusions record the state of magma throughout crystallisation: where varied inclusions show that the host magma body was compositionally heterogeneous, subsequent mixing acts to destroy this variability. There are many detailed studies of melt variability, especially from melt inclusions on Iceland (e.g. Gurenko and Chaussidon, 1995; Slater et al., 2001; Maclennan et al., 2003; Maclennan, 2008a,b; Neave et al., 2013, 2014), and the effect of mantle and crustal processes on this compositional heterogeneity is reasonably well understood. This provides an opportunity to compare our findings for CFB provinces with those from a well characterised system. It has been demonstrated that, in Iceland, higher Fo olivine that forms at an early stage of crystallisation in a cooling primitive magma has the potential to capture inclusions of initially heterogeneous primitive melt from the imperfect mixing of accumulated fractional melts. These melts are envisaged to have risen through porous channels in the mantle and accumulated and mixed in deep sill-like chambers near (above or below) the Moho (Maclennan, 2008a). Olivine which crystallises later traps inclusions of progressively more thoroughly mixed melts. This concurrent mixing and crystallisation is recorded in a reduction of melt inclusion variance with a reduction in host olivine Fo (Maclennan, 2008a).

To examine the evidence for this process in the present sample set, host olivine Fo is plotted against melt inclusion La/Yb as a proxy for all incompatible element variability in Fig. 11. La/Yb for a given inclusion is normalised to the mean of melt inclusions in the host whole-rock sample. This removes inter-sample offsets in La/Yb (e.g. as a consequence of differences in the extent of partial melting or crystallisation) and allows the variability of the relatively small number of inclusions from each sample to be considered together.

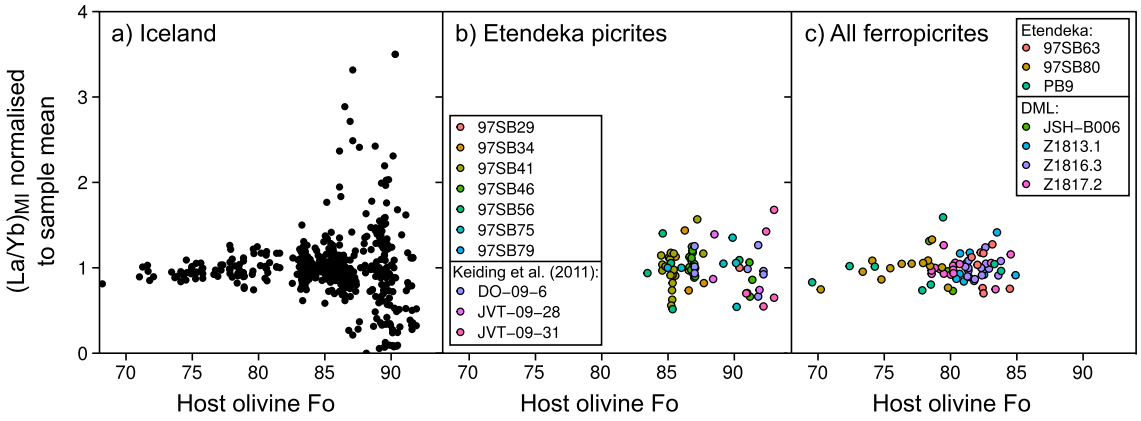

Fig. 11. La/Yb of individual melt inclusions normalised to the mean La/Yb of all melt inclusions plotted against host olivine Fo content for a given hand specimen from (a) Iceland (compilation of Maclennan, 2008a); (b) uncontaminated Etendeka picrites (this study and Keiding et al., 2011); (c) uncontaminated Etendeka and Antarctica ferropicrites, excluding samples 97SB67 and 97SB68. Colour of point corresponds to sample number.

Melt inclusion variability in Icelandic inclusions (Fig. 11a) is extremely large at high Fo contents (La/Yb ranges from 0 to 3.5 of the sample mean at $Fo_{>86}$) and funnels towards little variability at low Fo contents (La/Yb range of 0.7 to 1.3 of sample mean at $Fo_{<80}$). The reduction of variance with increased extent of crystallisation is clear. Statistics and M values shown in Table 1 were calculated for all inclusions in $Fo_{>82}$ olivines, so detail of the variance reduction with reducing Fo is lost. In this case, $M = 0.98$ reflects an average extent of mixing recorded by the inclusions; the highest Fo, highest variance inclusions would have a lower M value.

The Etendeka Horingbaai picrite melt inclusions occur in olivines with a compositional range of $Fo_{84–93}$, which is similar to that of the most variable Icelandic inclusions. However, the relative deviation of the Etendeka picrite inclusions at high Fo is much lower than that in the Icelandic samples (Fig. 11b). The observed La/Yb of individual inclusions range from 0.5 to 1.7 of the sample mean. The ferropicrites are similarly lacking in variability, especially at high Fo (note that the higher Fe/Mg of the primary melt means that the forsterite content of liquidus olivine is offset to lower values relative to picrite). In further contrast to Icelandic inclusions, the deviation from the mean of both Etendeka picrites and ferropicrites does not change systematically with forsterite content, so that rather than crystallisation-concurrent mixing occurring, the melts must have mixed to a greater extent prior to the onset of crystallisation.

Finally, we note that variable trace element and isotopic compositions are observed at all length scales in Iceland: melt inclusions with variable compositions are found within the same olivine; variable glass compositions are found within the same flow or volcanic centre (e.g. Maclennan et al., 2003; Stracke et al., 2003b; Maclennan, 2008a); and significant spatial variability of flow isotopic composition exists across the whole island (Shorttle et al., 2013). These observations are in contrast with the results of this study on CFB province rocks, where incompatible trace element contents of melt inclusions are homogeneous both within and between olivine grains. CFB provinces are characterised by large volumes of predominantly basaltic lava flows and intrusions. It follows that any variability observed within individual CFB lava flows (e.g. Vye-Brown et al., 2013) is not directly inherited from the primary melts; rather, it must be dominantly acquired through subsequent crustal processing such as assimilation, fractionation or mixing of different melt batches.

5.2.4. Controls on melt mixing and crystallisation in CFB provinces and the influence of tectonic setting

Fractional melts extracted at different depths in a melting column are expected to be compositionally heterogeneous (e.g. Sobolev and Shimizu, 1993; Gurenko and Chaussidon, 1995), and even more so if the mantle source consists of more than one lithology. The existence of both picrite and ferropicrite in the Paraná–Etendeka and Karoo CFB provinces shows that their mantle source regions consist of different lithologies (Gibson, 2002), so how do melts from a heterogeneous mantle result in homogeneous melt inclusion populations?

Initially-heterogeneous fractional mantle melts must have mixed to near completion prior to the liquidus temperature being reached, so that liquidus olivine is sampling a melt that has already homogenised. This mixing could happen both during transport through the mantle and within the deep crustal sills where these melts accumulate, as has been suggested for Iceland (Maclennan, 2008a). As shown in Table 1, primitive CFB melt inclusions on average represent 98.9% mixing prior to their entrapment, and Fig. 11b indicates that variance does not reduce with crystallisation, so that even the most primitive inclusions reflect this high level of mixing. The settings which produce the most homogeneous primitive inclusions tend to have a combination of thicker lithosphere and hotter mantle source (higher potential temperature, T_P); these conditions may provide a clue as to why their primitive melts are better mixed. The Etendeka picrites were generated by melting of peridotite at elevated mantle potential temperatures (1470–1560 °C) under a lithosphere of similar thickness (55–95 km; Thompson

et al., 2001) to that of some OIBs. The ferropicrites were also formed by melting at high mantle potential temperatures but may derive from deeper, lower fraction melting of garnet pyroxenite (Gibson, 2002; Tuff et al., 2005). At these conditions hot, high-MgO melts are produced.

One possibility is that these hot deep melts have a moderate superliquidus cooling interval when emplaced in the crust as a result of the large pressure drop that they experienced since their formation deep in the mantle. Instantaneous melts would follow a liquid adiabat when rising through lithosphere with a shallower PT gradient than the melt liquidus. Following aggregation in crustal sills, the superliquidus melt can then undergo convective mixing as it cools to its liquidus temperature. This could be the case for all melts formed under moderately thick lithosphere, contributing towards the higher degree of mixing observed in samples from thicker lithosphere settings (CFB and OIB; Fig. 10). The high melt flux in CFB provinces may also alter the geothermal gradient by warming the lower crust, reducing the rate at which magma bodies cool. Conversely, thinner lithosphere allows adiabatic decompression melting to shallower depths, resulting in a smaller pressure drop between melt production and crustal emplacement (so a smaller liquidus temperature overstep).

Differences in mantle potential temperature could also play a role by controlling the physical properties of the melts produced. High T_P melting produces hotter, more MgO-rich melts which are less viscous than the cooler, relatively MgO-poor melts produced by ambient T_P mantle. Lowering the viscosity will raise the Rayleigh number and promote convection, leading to an increased likelihood of vigorous convective mixing of melts from settings with high mantle potential temperatures. The physical properties of picrite and ferropicrite primary melts support convective mixing prior to the onset of crystallisation. At their respective liquidi, both picrite and ferropicrite melts have a lower dynamic viscosity than MORBs, and ferropicrite has a viscosity even lower than picrite. We performed calculations in MELTS (Ghiorso and Sack, 1995) which indicate that while the dynamic viscosity of primary MORB at liquidus temperatures at 1 kbar is 5.4 Pa s (composition calculated from Siqueros primitive MORB by Herzberg and Asimow, 2015), the viscosity of Etendeka ferropicrite (97SB63) and picrite (97SB33) at 5 kbar is 0.7 Pa s and 1.1 Pa s, respectively. Additionally, the most primitive olivines ($Fo_{>90}$) from the Etendeka picrites record a high mean Al-in-olivine crystallisation temperature of 1457 °C (Jennings, 2016, using the thermometer calibration of Coogan et al., 2014). The Ahlmannryggen ferropicrite olivines record a mean crystallisation temperature of 1279 °C (Heinonen et al., 2015), which is higher than the MORB mean obtained using the same thermometer (1195 °C, Coogan et al., 2014). These hot, low viscosity picritic and ferropicritic liquids could have experienced vigorous convection prior to the onset of crystallisation; such efficient mixing would cause melt inclusions to record a rather homogeneous melt composition.

We suggest that the thicker lithosphere and high temperature mantle source associated with intra-plate settings can promote melt mixing in magma chambers prior to and during crystallisation, promoting melt inclusion homogeneity. The Icelandic mantle source is also hot (~130 °C hotter than the MORB-source mantle; Shorttle et al., 2014), although Iceland lacks the thick lithospheric of the other settings, so decompression melting proceeds to shallower levels. MAR samples are the least homogeneous, perhaps as a result of their shallow melting regime.

It should also be considered that mixing of instantaneous melts begins during their segregation and transport, prior to emplacement in crustal or near-Moho sills. During adiabatic decompression melting, high-porosity channels are likely to form through reactive transport processes; these serve to segregate instantaneous melts close to their source and deliver compositionally heterogeneous melts to magma chambers (e.g. Spiegelman and Kelemen, 2003). In addition, lithological heterogeneity may promote the formation of a channelised flow regime (Katz and Weatherley, 2012 and Weatherley and Katz, 2012). However, prior to channel nucleation (i.e. at low melt fraction), melts may be trapped in situ, promoting equilibrium melting conditions and homogenisation. The extent to which channelised flow develops during the high pressure, low fraction melting that produces ferropicrites is likely to be limited, especially at pressures above the peridotite solidus where a significant permeability barrier may exist (Rudge et al., 2013). Although mixing probably occurs both during transport and after accumulation in crustal sills or chambers, the melt inclusion data cannot be used to determine the relative importance of the two; it simply indicates the state of the melt at the onset of crystallisation.

In summary, the high degree of melt inclusion homogeneity observed in the picrites and ferropicrites in this study may be related to their tectonic setting and mantle melting processes, and mixing of the primary mantle melts occurred almost entirely prior to the onset of crystallisation.

5.3. The lack of crustal assimilation in olivine-hosted melt inclusions from primitive Paraná–Etendeka and Karoo CFB melts

If the primitive melts studied here were effectively mixed in sill-like magma chambers within the continental crust, it is important to consider why they show only limited geochemical evidence of interaction with lithospheric materials, as indicated by the whole-rock data and melt inclusions. Spera and Bohrson (2001) provided energy-constrained assimilation–fractional crystallisation (EC–AFC) equations to estimate the thermodynamics of magmas that crystallise in contact with crustal wall-rocks. We perform such modelling in order to predict whether the melt parental to the Etendeka picrites is, in fact, expected to assimilate much crustal material. The model parameters and results are presented in Table 2.

To constrain the model parameters for the melt, we used the parental melt major element composition estimated for the Horingbaai picrites by Thompson and Gibson (2000) and a liquidus temperature of 1450 °C, which corresponds to the highest temperatures recorded in the Paraná–Etendeka picrites and other CFB province primitive

Table 2
EC–AFC modelling parameters and results.

Variable	PM	Upper crust (standard)	Upper crust (rift)	Lower crust (standard)	Lower crust (rift)
Magma liquidus T [°C]	1450	–	–	–	–
Magma initial T [°C]	1500	–	–	–	–
Assimilant liquidus T [°C]	–	1000	1000	1100	1100
Assimilant initial T [°C]	–	300	700	600	800
Solidus T [°C]	–	850	850	950	950
Equilibration T [°C]	–	980	980	1080	1080
Isobaric specific heat [J kg^{-1} K^{-1}]	1650	1370	1370	1388	1388
Crystallisation enthalpy [J kg^{-1}]	470,000	–	–	–	–
Fusion enthalpy [J kg^{-1}]	–	270,000	270,000	350,000	350,000
M_c/M_a at $M_a = 1$ wt.%	–	63	17	38	13

Sources for the parental melt (PM) parameters: magma liquidus based on Al-in-olivine crystallisation temperatures for LIP picrites (Coogan et al., 2014; Heinonen et al., 2015; Jennings, 2016); initial T is an illustrative example high T to demonstrate the effect of a superliquidus melt temperature; isobaric specific heat calculated on the basis of major element composition estimated for the Horingbaai parental melt (Thompson and Gibson, 2000) using the partial molar isobaric heat capacities listed by Spera and Bohrson (2001); crystallization enthalpy estimated using equilibrium crystallisation model for the major element composition at 5 kbar ($Cr_2O_3 = 0.5$ wt.%) using the MELTS model in the software PELE (Boudreau, 1999). Thermodynamic parameters represent the standard crustal values of Bohrson and Spera (2001) with additional modelling performed with initial temperatures compatible with active continental rift environment (see Bohrson and Spera (2001) and Heinonen et al. (2016)).

magmas by Al-in-olivine thermometry (Coogan et al., 2014; Heinonen et al., 2015; Jennings, 2016). To demonstrate the effect of a superliquidus melt temperature, the initial temperature of the melt was taken as 1500 °C. For the crustal wallrocks, we used the standard crustal parameters provided by Bohrson and Spera (2001), and performed additional calculations with initial contaminant temperatures that take into account the heating effect of mafic underplating in a continental rift environment (see Bohrson and Spera, 2001). Using high equilibration temperatures and high initial melt and contaminant temperatures ensures that the amount of crystallisation prior to initiation of wall-rock melting is not overestimated.

The models using standard and continental rift parameters for upper crust suggest that 63 and 17 wt.% of cumulates, respectively, may form before the high-T magma has experienced 1 wt.% of contamination (relative to initial mass of magma) from the wall rock. This allows ample opportunity for the mantle melts to mix and crystallise within the sills before crustal contamination takes place. This is equivalent to $M_a/M_c = 0.02$ and 0.06 (at $F = 0.99$) respectively, which is consistent with our observations from melt inclusions. The models are also compatible with the observation that picrites in CFBs tend to be uncontaminated whereas more evolved basalts and basaltic andesites with MgO of 4–6 wt.% often have a crustal overprint (e.g. Thompson, 1982), and again indicate that olivine-hosted melt inclusions can faithfully preserve a record of mantle melting processes, even when the host magma is emplaced in thick continental crust.

6. CONCLUSIONS

The major and trace element compositions of 154 olivine-hosted melt inclusions have been analysed from primitive rocks (picrites and ferropicrites) from the Paraná–Etendeka and Karoo CFB provinces. These melt inclusions were originally crystalline and their major element compositions have been altered during the re-homogenisation processes. In contrast, incompatible trace element compositions of the melt inclusions mirror those of their host rocks and small systematic variations reflect dilution processes, resulting from the addition or subtraction of olivine into the melt inclusion during homogenisation. This implies that whole-rock analyses for similar older, fully crystalline rocks can still provide a meaningful approximation of the initial liquid chemistry. Trace element compositions of most of our melt inclusions were largely unaffected by crustal contamination and only a small subset were breached prior to re-homogenisation. We conclude that the whole-rock incompatible trace element chemistry of these picrites and ferropicrites is a good approximation of the original liquid composition, and represents the well-mixed average of primary fractional mantle melts.

The olivine-hosted melt inclusions in the uncontaminated Etendeka picrites and ferropicrites are homogeneous, i.e. these mantle-derived melts were well mixed at the time of melt inclusion entrapment. High degrees of homogeneity in the incompatible trace element compositions of olivine-hosted melt inclusions also occur in datasets from global CFB provinces and OIB settings, where the lithosphere is moderately thick (i.e. >50 km) and adiabatic decompression melting is restricted to higher pressures. This contrasts with datasets from mid-ocean ridges (e.g. FAMOUS and 43° N on the Mid Atlantic Ridge and Iceland). The homogeneity in melt inclusions hosted in high-Fo olivine in CFB settings shows that the primitive melts from which olivine crystallised were already well mixed with respect to their source fractional melts by the onset of olivine crystallisation. In these settings, hot, high-MgO melts have been transported over a large depth range in the lithosphere and pooled in the crust at significantly lower pressures than those of their formation. The high and potentially superliquidus temperature together with the low viscosity of these liquids could promote the convective mixing of melts prior to entrapment in liquidus olivine. The increased melt flux in CFB settings and differences in melt physical properties may also play a role in promoting early mixing.

ACKNOWLEDGEMENTS

We thank Keith Putirka and two anonymous reviewers for their detailed and helpful comments, and Andreas Stracke for his additional remarks and editorial handling; all improved the clarity of our arguments and the presentation of this manuscript. We acknowledge Cees Jan De-Hoog for technical assistance and expertise at the NERC Ion Microprobe Facility at the University of Edinburgh, and Iris Buisman for assistance with the EPMA at the University of Cambridge. We are grateful to the scientists involved in the field expeditions during which samples used in this study were collected including: Bob Thompson, Paula Antoshechkina, Teal Riley, Philip Leat and Ilona Romu. This work was supported by a Natural Environment Research Council studentship [NE/J500070/1 to E.S.J.], Natural Environment Research Council funding for ion microprobe analysis [IMF460/0512 and IMF482/0513 to S.A.G.] and funding from the University of Cambridge.

APPENDIX A. SUPPLEMENTARY DATA

Supplementary data associated with this article can be found, in the online version, at http://dx.doi.org/10.1016/j.gca.2016.09.015.

REFERENCES

Arndt N. T., Czamanske G. K., Wooden J. L. and Fedorenko V. A. (1993) Mantle and crustal contributions to continental flood volcanism. *Tectonophysics* **223**, 39–52.

Bohrson W. A. and Spera F. J. (2001) Energy-constrained open-system magmatic processes ii: application of energy-constrained assimilation-fractional crystallization (EC–AFC) model to magmatic systems. *J. Petrol.* **42**, 1019–1041.

Boudreau A. E. (1999) PELE—a version of the MELTS software program for the PC platform. *Comput. Geosci.* **25**, 201–203.

Bryan S. E. and Ernst R. E. (2008) Revised definition of Large Igneous Provinces (LIPs). *Earth-Sci. Rev.* **86**, 175–202.

Coogan L. A., Saunders A. D. and Wilson R. N. (2014) Aluminum-in-olivine thermometry of primitive basalts: Evidence of an anomalously hot mantle source for large igneous provinces. *Chem. Geol.* **368**, 1–10.

Courtillot V. E. and Renne P. R. (2003) On the ages of flood basalt events. *Comptes Rendus Geosci.* **335**, 113–140.

Cox K. G. (1980) A model for flood basalt vulcanism. *J. Petrol.* **21**, 629–650.

Danyushevsky L. V. and Plechov P. (2011) Petrolog 3: integrated software for modeling crystallization processes. *Geochem. Geophys. Geosyst.* **12**, Q07021. http://dx.doi.org/10.1029/2011GC003516.

Danyushevsky L. V., Della-Pasqua F. N. and Sokolov S. (2000) Re-equilibration of melt inclusions trapped by magnesian olivine phenocrysts from subduction-related magmas: petrological implications. *Contrib. Mineral. Petrol.* **138**, 68–83.

Danyushevsky L. V., McNeill A. W. and Sobolev A. V. (2002) Experimental and petrological studies of melt inclusions in phenocrysts from mantle-derived magmas: an overview of techniques, advantages and complications. *Chem. Geol.* **183**, 5–24.

Danyushevsky L. V., Leslie R. A. J., Crawford A. J. and Durance P. (2004) Melt inclusions in primitive olivine phenocrysts: the role of localized reaction processes in the origin of anomalous compositions. *J. Petrol.* **45**, 2531–2553.

Davis F. A., Hirschmann M. M. and Humayun M. (2011) The composition of the incipient partial melt of garnet peridotite at 3 GPa and the origin of OIB. *Earth Planet. Sci. Lett.* **308**, 380–390.

DePaolo D. J. (1981) Trace element and isotopic effects of combined wallrock assimilation and fractional crystallization. *Earth Planet. Sci. Lett.* **53**, 189–202.

Erlank A. J., Marsh J. S., Duncan A. R., Miller R. M., Hawkesworth C. J., Betton P. J. and Rex D. C. (1984) Geochemistry and petrogenesis of the Etendeka volcanic rocks from SWA/Namibia. In *Petrogenesis of the Volcanic Rocks of the Karoo Province Geological Society of South Africa: Special publication*. Geological Society of South Africa, pp. 195–245.

Gaetani G. and Watson E. (2000) Open system behavior of olivine-hosted melt inclusions. *Earth Planet. Sci. Lett.* **183**, 27–41.

Ghiorso M. S. and Sack R. O. (1995) Chemical mass transfer in magmatic processes IV. A revised and internally consistent thermodynamic model for the interpolation and extrapolation of liquid–solid equilibria in magmatic systems at elevated temperatures and pressures. *Contrib. Mineral. Petrol.* **119**, 197–212.

Gibson S. A. (2002) Major element heterogeneity in Archean to Recent mantle plume starting-heads. *Earth Planet. Sci. Lett.* **195**, 59–74.

Gibson S. A. and Geist D. (2010) Geochemical and geophysical estimates of lithospheric thickness variation beneath Galápagos. *Earth Planet. Sci. Lett.* **300**, 275–286.

Gibson S. A., Thompson R. N. and Dickin A. P. (2000) Ferropicrites: geochemical evidence for Fe-rich streaks in upwelling mantle plumes. *Earth Planet. Sci. Lett.* **174**, 355–374.

Gibson S. A., Thompson R. N. and Day J. A. (2006) Timescales and mechanisms of plume–lithosphere interactions: 40Ar/39Ar geochronology and geochemistry of alkaline igneous rocks from the Paraná–Etendeka large igneous province. *Earth Planet. Sci. Lett.* **251**, 1–17.

Gurenko A. and Chaussidon M. (1995) Enriched and depleted primitive melts included in olivine from Icelandic tholeiites: origin by continuous melting of a single mantle column. *Geochim. Cosmochim. Acta* **59**, 2905–2917.

Harris C., Roux P., Le Cochrane R., Martin L., Duncan A. R., Marsh J. S., Le Roex A. P. and Class C. (2015) The oxygen isotope composition of Karoo and Etendeka picrites: High $\delta^{18}O$ mantle or crustal contamination? *Contrib. Mineral. Petrol.* **170**, 1–24.

Heinonen J. S. and Luttinen A. V. (2008) Jurassic dikes of Vestfjella, western Dronning Maud Land, Antarctica: geochemical tracing of ferropicrite sources. *Lithos* **105**, 347–364.

Heinonen J. S., Carlson R. W. and Luttinen A. V. (2010) Isotopic (Sr, Nd, Pb, and Os) composition of highly magnesian dikes of Vestfjella, western Dronning Maud Land, Antarctica: a key to the origins of the Jurassic Karoo large igneous province? *Chem. Geol.* **277**, 227–244.

Heinonen J. S., Luttinen A. V., Riley T. R. and Michallik R. M. (2013) Mixed pyroxenite–peridotite sources for mafic and ultramafic dikes from the Antarctic segment of the Karoo continental flood basalt province. *Lithos* **177**, 366–380.

Heinonen J. S., Carlson R. W., Riley T. R., Luttinen A. V. and Horan M. F. (2014) Subduction-modified oceanic crust mixed with a depleted mantle reservoir in the sources of the Karoo continental flood basalt province. *Earth Planet. Sci. Lett.* **394**, 229–241.

Heinonen J. S., Jennings E. S. and Riley T. R. (2015) Crystallisation temperatures of the most Mg-rich magmas of the Karoo LIP on the basis of Al-in-olivine thermometry. *Chem. Geol.* **411**, 26–35.

Heinonen J. S., Luttinen A. V. and Bohrson W. A. (2016) Enriched continental flood basalts from depleted mantle melts: modeling the lithospheric contamination of Karoo lavas from Antarctica. *Contrib. Mineral. Petrol.* **171**, 9.

Herzberg C. and Asimow P. D. (2015) PRIMELT3 MEGA.XLSM software for primary magma calculation: peridotite primary magma MgO contents from the liquidus to the solidus. *Geochem. Geophys. Geosyst.* **16**, 563–578. http://dx.doi.org/10.1002/2014GC005631.

Herzberg C. and O'Hara M. J. (2002) Plume-associated ultramafic magmas of Phanerozoic age. *J. Petrol.* **43**, 1857–1883.

Jackson M. G. and Hart S. R. (2006) Strontium isotopes in melt inclusions from Samoan basalts: implications for heterogeneity in the Samoan plume. *Earth Planet. Sci. Lett.* **245**, 260–277.

Jackson M. G., Cabral R. A., Rose-Koga E. F., Koga K. T., Price A., Hauri E. H. and Michael P. (2015) Ultra-depleted melts in olivine-hosted melt inclusions from the Ontong Java Plateau. *Chem. Geol.* **414**, 124–137.

Jennings E. S. (2016) *Ferropicrites as evidence for lithological heterogeneity in the mantle source of continental flood basalts* (PhD thesis). University of Cambridge.

Jochum K. P., Nohl U., Herwig K., Lammel E., Stoll B. and Hofmann A. W. (2005) GeoReM: a new geochemical database for reference materials and isotopic standards. *Geostand. Geoanal. Res.* **29**, 333–338.

Jochum K. P., Weis U., Stoll B., Kuzmin D., Yang Q., Raczek I., Jacob D. E., Stracke A., Birbaum K., Frick D. A., Günther D. and Enzweiler J. (2011) Determination of reference values for NIST SRM 610–617 glasses following ISO guidelines. *Geostand. Geoanal. Res.* **35**, 397–429.

Jourdan F., Féraud G., Bertrand H., Kampunzu A. B., Tshoso G., Watkeys M. K. and Gall B. L. (2005) Karoo large igneous province: brevity, origin, and relation to mass extinction questioned by new 40Ar/39Ar age data. *Geology* **33**, 745–748.

Kamenetsky V. S., Eggins S. M., Crawford A. J., Green D. H., Gasparon M. and Falloon T. J. (1998) Calcic melt inclusions in primitive olivine at 43°N MAR: evidence for melt–rock reaction/melting involving clinopyroxene-rich lithologies during MORB generation. *Earth Planet. Sci. Lett.* **160**, 115–132.

Kamenetsky V. S., Chung S.-L., Kamenetsky M. B. and Kuzmin D. V. (2012) Picrites from the Emeishan Large Igneous Province, SW China: a compositional continuum in primitive magmas and their respective mantle sources. *J. Petrol.* **53**, 2095–2113.

Katz R. F. and Weatherley S. M. (2012) Consequences of mantle heterogeneity for melt extraction at mid-ocean ridges. *Earth Planet. Sci. Lett.* **335–336**, 226–237.

Keiding J., Trumbull R., Veksler I. and Jerram D. (2011) On the significance of ultra-magnesian olivines in basaltic rocks. *Geology* **39**, 1095–1098.

Kent A. J. R., Baker J. A. and Wiedenbeck M. (2002) Contamination and melt aggregation processes in continental flood basalts: constraints from melt inclusions in Oligocene basalts from Yemen. *Earth Planet. Sci. Lett.* **202**, 577–594.

Kirstein L. A., Kelley S., Hawkesworth C., Turner S., Mantovani M. and Wijbrans J. (2001) Protracted felsic magmatic activity associated with the opening of the South Atlantic. *J. Geol. Soc.* **158**, 583–592.

Kogiso T., Hirose K. and Takahashi E. (1998) Melting experiments on homogeneous mixtures of peridotite and basalt: application to the genesis of ocean island basalts. *Earth Planet. Sci. Lett.* **162**, 45–61.

Koleszar A. M., Saal A. E., Hauri E. H., Nagle A. N., Liang Y. and Kurz M. D. (2009) The volatile contents of the Galapagos plume; evidence for H2O and F open system behavior in melt inclusions. *Earth Planet. Sci. Lett.* **287**, 442–452.

Kreissig K., Nägler T. F., Kramers J. D., van Reenen D. D. and Smit C. A. (2000) An isotopic and geochemical study of the northern Kaapvaal Craton and the Southern Marginal Zone of the Limpopo Belt: are they juxtaposed terranes? *Lithos* **50**, 1–25.

Kress V. C. and Carmichael I. S. E. (1991) The compressibility of silicate liquids containing Fe_2O_3 and the effect of composition, temperature, oxygen fugacity and pressure on their redox states. *Contrib. Mineral. Petrol.* **108**, 82–92.

Laubier M., Gale A. and Langmuir C. H. (2012) Melting and crustal processes at the FAMOUS segment (Mid-Atlantic Ridge): new insights from olivine-hosted melt inclusions from multiple samples. *J. Petrol.* **53**, 665–698.

Le Bas M. J. (2000) IUGS reclassification of the High-Mg and picritic volcanic rocks. *J. Petrol.* **41**, 1467–1470.

Luttinen A. V., Heinonen J. S., Kurhila M., Jourdan F., Mänttäri I., Vuori S. K. and Huhma H. (2015) Depleted mantle-sourced CFB magmatism in the Jurassic Africa-Antarctica rift: Petrology and 40Ar/39Ar and U/Pb chronology of the Vestfjella dyke swarm, Dronning Maud Land, Antarctica. *J. Petrol.*, egv022.

Maclennan J. (2008a) Concurrent mixing and cooling of melts under Iceland. *J. Petrol.* **49**, 1931–1953.

Maclennan J. (2008b) Lead isotope variability in olivine-hosted melt inclusions from Iceland. *Geochim. Cosmochim. Acta* **72**, 4159–4176.

Maclennan J., McKenzie D., Hilton F., Gronvold K. and Shimizu N. (2003) Geochemical variability in a single flow from northern Iceland. *J. Geophys. Res.* **108**, 2007.

Marsh J. S., Ewart A., Milner S. C., Duncan A. R. and Miller R. M. (2001) The Etendeka Igneous Province: Magma types and their stratigraphic distribution with implications for the evolution of the Paraná-Etendeka flood basalt province. *B Volcanol.* **62**, 464–486.

Marschall H. R., Hawkesworth C. J., Storey C. D., Dhuime B., Leat P. T., Meyer H.-P. and Tamm-Buckle S. (2010) The Annandagstoppane Granite, East Antarctica: Evidence for Archaean intracrustal recycling in the Kaapvaal-Grunehogna craton from zircon O and Hf isotopes. *J. Petrol.* **51**, 2277–2301.

Matzen A. K., Baker M. B., Beckett J. R. and Stolper E. M. (2011) Fe–Mg partitioning between olivine and high-magnesian melts and the nature of Hawaiian parental liquids. *J. Petrol.* **52**, 1243–1263.

McDonough W. F. and Sun S.-S. (1995) The composition of the Earth. *Chem. Geol.* **120**, 223–253.

Neave D. A., Passmore E., Maclennan J., Fitton G. and Thordarson T. (2013) Crystal–melt relationships and the record of deep mixing and crystallization in the ad 1783 Laki eruption, Iceland. *J. Petrol.* **54**, 1661–1690.

Neave D. A., Maclennan J., Hartley M. E., Edmonds M. and Thordarson T. (2014) Crystal storage and transfer in basaltic systems: the Skuggafjöll eruption, Iceland. *J. Petrol.* **55**, 2311–2346.

Nielsen T. F. D., Turkov V. A., Solovova I. P., Kogarko L. N. and Ryabchikov I. D. (2006) A Hawaiian beginning for the Iceland plume: Modelling of reconnaissance data for olivine-hosted melt inclusions in Palaeogene picrite lavas from East Greenland. *Lithos* **92**, 83–104.

Nielsen R. L., Michael P. J. and Sours-Page R. (1998) Chemical and physical indicators of compromised melt inclusions. *Geochim. Cosmochim. Acta* **62**, 831–839.

Norman M. D., Garcia M. O., Kamenetsky V. S. and Nielsen R. L. (2002) Olivine-hosted melt inclusions in Hawaiian picrites: equilibration, melting, and plume source characteristics. *Chem. Geol.* **183**, 143–168.

Peate D. W., Peate I. U., Rowe M. C., Thompson J. M. and Kerr A. C. (2012) Petrogenesis of high-MgO lavas of the Lower Mull

Plateau Group, Scotland: Insights from melt inclusions. *J. Petrol.* **53**, 1867–1886.

Pertermann M., Hirschmann M. M., Hametner K., Günther D. and Schmidt M. W. (2004) Experimental determination of trace element partitioning between garnet and silica-rich liquid during anhydrous partial melting of MORB-like eclogite. *Geochem. Geophys. Geosyst.* **5**, Q05A01. http://dx.doi.org/10.1029/2003GC000638.

Reidel S. P. and Tolan T. L. (2013) The Grande Ronde Basalt, Columbia River Basalt Group. In *Geological Society of America Special Papers*, Vol. 497, pp. 117–153.

Renne P. R., Glen J. M., Milner S. C. and Duncan A. R. (1996) Age of Etendeka flood volcanism and associated intrusions in southwestern Africa. *Geology* **24**, 659–662.

Richards M. A., Duncan R. A. and Courtillot V. E. (1989) Flood basalts and hot-spot tracks: Plume heads and tails. *Science* **246**, 103–107.

Riley T. R., Leat P. T., Curtis M. L., Millar I. L., Duncan R. A. and Fazel A. (2005) Early-middle Jurassic dolerite dykes from western Dronning Maud Land (Antarctica): identifying mantle sources in the Karoo Large Igneous Province. *J. Petrol.* **46**, 1489–1524.

Rowe M. C. (2006) Anomalously high Fe contents in rehomogenized olivine-hosted melt inclusions from oxidized magmas. *Am. Mineral.* **91**, 82–91.

Rudge J. F., Maclennan J. and Stracke A. (2013) The geochemical consequences of mixing melts from a heterogeneous mantle. *Geochim. Cosmochim. Acta* **114**, 112–143.

Rudnick R. L. and Fountain D. M. (1995) Nature and composition of the continental crust: a lower crustal perspective. *Rev. Geophys.* **33**, 267–309.

Saal A. E., Hart S. R., Shimizu N., Hauri E. H. and Layne G. D. (1998) Pb isotopic variability in melt inclusions from oceanic island basalts, Polynesia. *Science* **282**, 1481–1484.

Sakyi P. A., Tanaka R., Kobayashi K. and Nakamura E. (2012) Inherited Pb isotopic records in olivine antecryst-hosted melt inclusions from Hawaiian lavas. *Geochim. Cosmochim. Acta* **95**, 169–195.

Salters V. J. M. and Stracke A. (2004) Composition of the depleted mantle. *Geochem. Geophys. Geosyst.* **5**, Q05B07. http://dx.doi.org/10.1029/2003GC000597.

Sarbas B. and Nohl U. (2008) The GEOROC database as part of a growing geoinformatics network. In *Proceedings: U.S. Geological Survey Scientific Investigations Report 2008–5172 Geoinformatics 2008—Data to Knowledge*. pp. 42–43.

Schmitt A. K., Emmermann R., Trumbull R. B., Bühn B. and Henjes-Kunst F. (2000) Petrogenesis and 40Ar/39Ar geochronology of the Brandberg Complex, Namibia: evidence for a major mantle contribution in metaluminous and peralkaline granites. *J. Petrol.* **41**, 1207–1239.

Shimizu N. (1998) The geochemistry of olivine-hosted melt inclusions in a FAMOUS basalt ALV519-4-1. *Phys. Earth Planet. Inter.* **107**, 183–201.

Shorttle O., Maclennan J. and Piotrowski A. M. (2013) Geochemical provincialism in the Iceland plume. *Geochim. Cosmochim. Acta* **122**, 363–397.

Shorttle O., Maclennan J. and Lambart S. (2014) Quantifying lithological variability in the mantle. *Earth Planet. Sci. Lett.* **395**, 24–40.

Sides I. R., Edmonds M., Maclennan J., Swanson D. A. and Houghton B. F. (2014) Eruption style at Kilauea Volcano in Hawai/'i linked to primary melt composition. *Nat. Geosci.* **7**, 464–469.

Slater L., McKenzie D., Grönvold K. and Shimizu N. (2001) Melt generation and movement beneath Theistareykir, NE Iceland. *J. Petrol.* **42**, 321–354.

Sobolev A. V. (1996) Melt inclusions in minerals as a source of principle petrological information. *Petrology* **4**, 228–239.

Sobolev A. V. and Shimizu N. (1993) Ultra-depleted primary melt included in an olivine from the Mid-Atlantic Ridge. *Nature* **363**, 151–154.

Sobolev A. V., Hofmann A. W. and Nikogosian I. K. (2000) Recycled oceanic crust observed in "ghost plagioclase" within the source of Mauna Loa lavas. *Nature* **404**, 986–990.

Sobolev A. V., Krivolutskaya N. A. and Kuzmin D. V. (2009) Petrology of the parental melts and mantle sources of Siberian trap magmatism. *Petrology* **17**, 253–286.

Sobolev A. V., Hofmann A. W., Jochum K. P., Kuzmin D. V. and Stoll B. (2011) A young source for the Hawaiian plume. *Nature* **476**, 434–437.

Sours-Page R., Nielsen R. L. and Batiza R. (2002) Melt inclusions as indicators of parental magma diversity on the northern East Pacific Rise. *Chem. Geol.* **183**, 237–261.

Spera F. J. and Bohrson W. A. (2001) Energy-constrained open-system magmatic processes I: general model and energy-constrained assimilation and fractional crystallization (EC–AFC) formulation. *J. Petrol.* **42**, 999–1018.

Spiegelman M. and Kelemen P. B. (2003) Extreme chemical variability as a consequence of channelized melt transport. *Geochem. Geophys. Geosyst.* **4**(1055). http://dx.doi.org/10.1029/2002GC000336.

Starkey N. A., Fitton J. G., Stuart F. M. and Larsen L. M. (2012) Melt inclusions in olivines from early Iceland plume picrites support high 3He/4He in both enriched and depleted mantle. *Chem. Geol.* **306–307**, 54–62.

Stracke A., Bizimis M. and Salters V. J. M. (2003a) Recycling oceanic crust: quantitative constraints. *Geochem. Geophys. Geosyst.* **4**, 8003. http://dx.doi.org/10.1029/2001GC000223.

Stracke A., Zindler A., Salters V. J. M., McKenzie D., Blichert-Toft J., Albarède F. and Grönvold K. (2003b) Theistareykir revisited. *Geochem. Geophys. Geosyst.* **4**, 8507. http://dx.doi.org/10.1029/2002GC000347.

Thompson R. N. (1982) Magmatism of the British Tertiary Volcanic Province. *Scott. J. Geol.* **18**, 49–107.

Thompson R. N. and Gibson S. A. (2000) Transient high temperatures in mantle plume heads inferred from magnesian olivines in Phanerozoic picrites. *Nature* **407**, 502–506.

Thompson R. N., Gibson S. A., Dickin A. P. and Smith P. M. (2001) Early Cretaceous basalt and picrite dykes of the southern Etendeka region, NW Namibia: windows into the role of the Tristan mantle plume in Paraná–Etendeka magmatism. *J. Petrol.* **42**, 2049–2081.

Thompson R. N., Riches A. J. V., Antoshechkina P. M., Pearson D. G., Nowell G. M., Ottley C. J., Dickin A. P., Hards V. L., Nguno A.-K. and Niku-Paavola V. (2007) Origin of CFB magmatism: Multi-tiered intracrustal picrite-rhyolite magmatic plumbing at Spitzkoppe, western Namibia, during early Cretaceous Etendeka magmatism. *J. Petrol.* **48**, 1119–1154.

Tuff J. and Gibson S. A. (2007) Trace-element partitioning between garnet, clinopyroxene and Fe-rich picritic melts at 3 to 7 GPa. *Contrib. Mineral. Petrol.* **153**, 369–387.

Tuff J., Takahashi E. and Gibson S. A. (2005) Experimental constraints on the role of garnet pyroxenite in the genesis of high-Fe mantle plume derived melts. *J. Petrol.* **46**, 2023–2058.

Vye-Brown C., Gannoun A., Barry T. L., Self S. and Burton K. W. (2013) Osmium isotope variations accompanying the eruption

of a single lava flow field in the Columbia River Flood Basalt Province. *Earth Planet. Sci. Lett.* **368**, 183–194.

Weatherley S. M. and Katz R. F. (2012) Melting and channelized magmatic flow in chemically heterogeneous, upwelling mantle. *Geochem. Geophys. Geosyst.* **13**, Q0AC18. http://dx.doi.org/10.1029/2011GC003989.

White R. and McKenzie D. (1989) Magmatism at rift zones: the generation of volcanic continental margins and flood basalts. *J. Geophys. Res. Solid Earth* **94**, 7685–7729.

Wooden J. L., Czamanske G. K., Fedorenko V. A., Arndt N. T., Chauvel C., Bouse R. M., King B.-S. W., Knight R. J. and Siems (1993) Isotopic and trace-element constraints on mantle and crustal contributions to Siberian continental flood basalts, Noril'sk area, Siberia. *Geochim. Cosmochim. Acta* **57**, 3677–3704.

Yaxley G. M., Kamenetsky V. S., Kamenetsky M., Norman M. D. and Francis D. (2004) Origins of compositional heterogeneity in olivine-hosted melt inclusions from the Baffin Island picrites. *Contrib. Mineral. Petrol.* **148**, 426–442.

Associate editor: Andreas Stracke